Measurement and results; two aspects of a bubble chamber experiment

PART B

A STUDY OF THE $K^-\pi^-$ ELASTIC SCATTERING

Henk Voorthuis

UNIVERSITEIT VAN AMSTERDAM
ZEEMAN-LABORATORIUM

MEASUREMENT AND RESULTS; TWO ASPECTS OF A BUBBLE CHAMBER EXPERIMENT

PART A A SYSTEM FOR ON-LINE MEASUREMENT OF BUBBLE CHAMBER PHOTOGRAPHS, USING ENETRA MEASUREMENT DEVICES

PART B A STUDY OF THE $K^-\pi^-$ ELASTIC SCATTERING

Academisch proefschrift

ter verkrijging van de graad van doctor in de wiskunde en natuurwetenschappen aan de Universiteit van Amsterdam, op gezag van de rector magnificus, Dr. A. de Froe hoogleraar in de faculteit der Geneeskunde, in het openbaar te verdedigen in de aula der Universiteit (tijdelijk in de Lutherse Kerk, ingang Singel 411, hoek Spui) op woensdag 4 april 1973, des namiddags te 4 uur.

door

HENDRIK VOORTHUIS

geboren te Oegstgeest

1973

Typewerk verzorgd door Academic Service, Dodaarslaan 95, Vinkeveen

PROMOTOR: Prof. Dr. A.G.C. TENNER

The work described in this thesis has been performed in the "Zeeman laboratorium" of the University of Amsterdam as part of the research program of the "Stichting voor Fundamenteel Onderzoek der Materie (F.O.M.)", which is financially supported by the "Nederlandse Organisatie voor Zuiver Wetenschappelijk Onderzoek (Z.W.O.)".

Aan mijn ouders

Aan mijn vrouw

CONTENTS OF PART B

CONTENTS OF PART A

PART B

A STUDY OF THE $K^-\pi^-$ ELASTIC SCATTERING

A STUDY OF THE $K^-\pi^-$ ELASTIC SCATTERING

4.1 INTRODUCTION

In order to understand the role of the spin zero π and K mesons in the interaction of hadrons, the $\pi\pi$ and $K\pi$ interactions have been studied in many experiments. Since K or π meson targets are not available, information on the $\pi\pi$ and $K\pi$ interactions can only be obtained indirectly.

Earlier investigations have led to the identification and study of $K\pi$ resonances in the low energy region[4.1]. There is also information on the determination of the cross section and the phase shift analyses of the elastic $\pi\pi$ and $K\pi$ scattering not restricted to the resonance region[4.2]. In addition, the inelastic $\pi\pi$ and $K\pi$ scattering is under investigation[4.3].

Most of the analyses of the elastic $K\pi$ scattering have been done in the channels $K^{\pm}\pi^{\mp} \rightarrow K^{\pm}\pi^{\mp}$ and $K^{\pm}\pi^{\mp} \rightarrow K^{0}\pi^{0}$ [4.4, 4.2]. In these experiments the isospin I = 1/2 $K^*(890)$ resonance dominates at low energy. From the experimental relation $\sigma(K^+\pi^- \rightarrow K^+\pi^-) \approx 2\sigma(K^+\pi^- \rightarrow K^0\pi^0)$ as has been found in the analysis of the reactions $K^+ + p \rightarrow K^{+}_{0} + \pi^{0} + \Delta^{++}(1236)$ at 7.3 GeV/c [4.5], it may be concluded that the I = 3/2 $K\pi$ scattering amplitude is small compared to the I = 1/2 scattering amplitude in the mass region considered. On the other hand, comparison of the moments of the $K\pi$ angular distribution in the $K\pi$ rest system for these reactions, suggests the existence of a non-zero I = 3/2 s-wave phase shift[4.6].

In order to study the isospin I = 3/2 elastic $K\pi$ scattering amplitude without the influence of a dominating isospin I = 1/2 $K\pi$ scattering, several experimentalists have started to study the $K^{\pm}\pi^{\pm} \rightarrow K^{\pm}\pi^{\pm}$ channels[4.7].

In this study the isospin I = 3/2 elastic scattering has been analysed using the reaction

$$K^- + p \rightarrow K^- + \pi^- + \Delta^{++}(1236) \qquad (4.1.1)$$

Among the four-prong four-constraints-fit events, this reaction has a prominent cross section and seems, therefore, a good channel to study the isospin I = 3/2 elastic $K^-\pi^-$ scattering.

Under the assumption that the one-pion-exchange mechanism is dominant in reaction 4.1.1, the elastic $K^-\pi^-$ cross section has been determined as a function of the $K^-\pi^-$ effective mass (sect. 4.3). For this purpose an extrapolation procedure has been used following the suggestions of G.F. Chew and F.E. Low[4.8]. The results are summarized in table 4.3.3 and in figure 4.3.4.

Further, the scattering angles of the final K^- meson in the $K^-\pi^-$ rest system have been studied, resulting in an attempt to obtain the $K^-\pi^-$ phase shifts (sect. 4.4 and 4.5). The results for the s- and p-wave phase shifts obtained from the elastic $K^-\pi^-$ cross section and the off-mass-shell moments are summarized in table 4.4.2 and figure 4.4.6. The moments have also been extrapolated to the pion pole. The results for the phase shifts obtained with the use of the extrapolated moments are summarized in table 4.5.2 and figure 4.5.11.

The events of the reaction 4.1.1 are a sub-sample of the sample of events which have been identified as the reaction

$$K^- + p \rightarrow K^- + \pi^- + p + \pi^+ \qquad (4.1.2)$$

The experiment has been done by exposing the 2 m CERN bubble chamber, filled with liquid hydrogen, to K^- mesons of 4.2 GeV/c momentum, from the m6 beam.

4.2 SAMPLE OF EVENTS

4.2.1 SAMPLE OF THE REACTION $K^- + p \rightarrow K^- + \pi^- + p + \pi^+$.

At the moment of analysis there were 39,000 four-prong events available on the Data Summary Tapes (DST). From this sample, 10,695 events have been identified by the kinematic reconstruction program GRIND as belonging to the reaction 4.1.2.

The sample of 10,695 events contains 9730 unique fits (91.0%) and 965 ambiguous fits (9.0%). - In the cases where the four-constraints fit for reaction 4.1.2 was ambiguous with a fit for another reaction, including a neutral particle,

the four-constraints fit was chosen (4C-fit rule). - The ambiguities are due to the inability to distinguish a K^- from a π^- meson by comparing the ionisation in the present experimental conditions. A decision is made by choosing the solution with the smallest chi-squared.
In the sample of four-prong events with a visible decaying negative particle, 351 events fit the reaction 4.1.2 uniquely with a visible decaying K^- meson. These events have also been used for the analysis, making a total sample of 11,046 events for the reaction 4.1.2.

4.2.2 CROSS SECTION OF THE REACTION $K^- + p \rightarrow K^- + \pi^- + p + \pi^+$.

In this K^-p experiment the cross sections of the different reaction channels are determined using the observed number of tau-disintegrations within the fiducial volume. The total K^-p scattering cross section of this experiment, using the tau-callibration, σ_{K^-p} (4.2 GeV/c) = (25.8 ± 1.0)mb[4.9] is in agreement with the corresponding value obtained from counter experiments (25.5 ± 0.2)mb[4.10].
The cross section of a reaction is given by:

$$\sigma_T = N_T \frac{F_\tau}{N_\tau} \frac{m_K c^2}{pc.c\tau_K} \frac{M}{A\rho} \qquad (4.2.1)$$

in which:

N_T is the number of events of the relevant reaction within the fiducial volume (N_τ and N_T deal with the same sample of events.);

F_τ is the branching ratio for the tau-decay (= 0.0558 ± 0.0003[4.11]);

N_τ is the number of tau-disintegrations within the fiducial volume;

$\frac{pc}{m_K c^2} . c\tau_K$ is the mean decay length of the K^- meson;

c is the velocity of light (= 2.9979 x 10^{10}cm/sec);

p is the mean momentum of the incoming K^- meson (= (4.24 ± 0.04)GeV/c[4.12]); the experiment is carried out in several exposures of the bubble chamber, which results in slightly different beam momenta per exposure;

m_K is the mass of the K^- meson (= (493.84 ± 0.11)MeV/c^2 [4.11]);

τ_K is the life time of the K^- meson (= (1.2371 ± 0.0026)10^{-8}sec[4.11]);

$\frac{A\rho}{M}$ is the number of target particles (hydrogen) per cm^3;

A is the number of Avogadro (= 6.0222 x 10^{23} $mole^{-1}$; C_{12}-system);

ρ is the density of the hydrogen liquid (= 0.0622 g/cm^3 in the expanded stage[4.13]);

M is the atomic weight of the proton (= 1.008; C_{12}-system).

Since the sample mentioned in section 4.2.1 is not yet completely analysed, a sub-sample is used for the determination of the cross section of reaction 4.1.2. In this sub-sample, 7830 four-prong events (denoted as 400) and 227 four-prong events with a visible decaying K^- meson (410^-) are identified as belonging to the reaction 4.1.2.

These numbers must be corrected for the rejected events in the relevant topologies which contribute to the cross section. It is assumed that, within a certain topology, the rejected events may be distributed in proportion to the identified events over:

a. the events inside and outside the fiducial volume;
b. the events per reaction channel.

The rejected events may be classified in four main categories:

1. events which have been found in the scanning process, but which for some reason have not been measured (e.g., events which have a short straight outgoing track) and events which did not yield a reasonable fit (category "NO FIT");
2. events that yielded more than two fits ("TOO MANY FITS");
3. events which have been lost by magnetic tape failures or in the book-keeping process ("LOST");
4. events which are transferred for further investigation (mainly recalculation by THRESH, GRIND or ZEEMEEL (MILLSTONE)).

The correction percentages, which are the average results of the evaluation of the data at two laboratories and of three exposures of the bubble chamber, are summarized in table 4.2.1.

Table 4.2.1 Correction percentages to be applied to the number of identified four-prong events in order to determine the cross section. The correction applied to the reaction $K^- + p \rightarrow K^- + \pi^- + p + \pi^+$ does not contain the correction for events with too many fits because of the "4C-fit rule" (sect. 4.2.1)

NO FIT	TOO MANY FITS	LOST	FURTHER INVESTIGATION	CORRECTION FOUR-PRONGS	CORRECTION $K^-p \rightarrow K^-\pi^-p\pi^+$
9.2 %	0.7 %	2.4 %	3.1 %	15.4 %	14.7 %

The assumption that rejected events may be divided proportionally to the identified events over the reaction channels will certainly not hold for

topologies with visible decaying particles. For example, a relatively large number of events with a short track of the decaying particle contributes to the sample of rejected events. In the sample of short-track decays, the decays of the Σ^- and Ξ^- mesons are favoured due to the fact that their life-time is short compared to that of the K^- meson.

A correction as deduced from the reject categories of the topology 410^- will be caused mainly by the characteristics of the Σ^- mesons. As mentioned above, these characteristics are different for the K^- mesons. It was, therefore, considered better to apply the overall reject-correction factor 14.7% to the reaction 4.1.2. Thus the corrected number of events of reaction 4.1.2 is $N_T = (7830 + 227) \times 1.147 = 9241$.

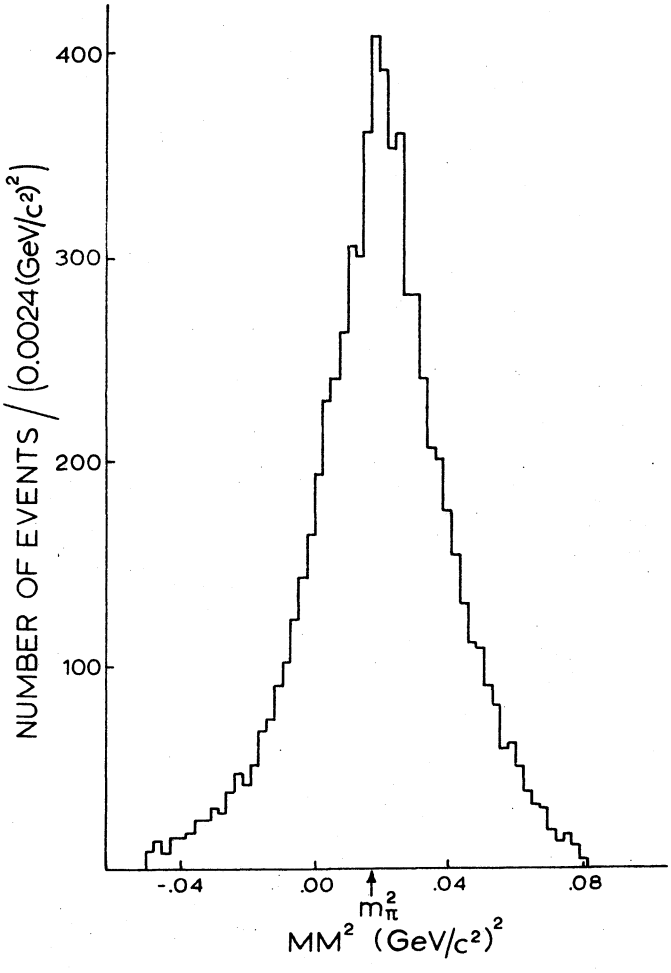

Figure 4.2.1 The spectrum of the missing mass to $K^-\pi^-p\pi^+$ in the reaction $K^- + p \rightarrow K^- + \pi^- + p + \pi^+ + \pi^o$.

It has also been investigated whether events which should yield the four-constraints fit of reaction 4.1.2, but for which this fit failed, have wrongly been classified in the one-constraint-fit categories. For this purpose the missing mass spectra of the one-constraint-fit reactions have been studied; e.g., the missing mass spectrum for the reaction $K^- + p \rightarrow K^- + \pi^- + p + \pi^+ + \pi^0$ is shown in figure 4.2.1. These spectra indicate that there is no large amount of events belonging to the four-constraints-fit reaction 4.1.2 which have wrongly been interpreted as belonging to the one-constraint-fit reactions.
The number of events which fit the hypothesis of the τ-decay is 93.6% of the number of scanned three-prong events[4.14]. This leads to the number of τ-decays: $N_\tau = 3403$.
The result for the total cross section of reaction 4.1.2 is

$$\sigma_{K^-p \rightarrow K^-\pi^-p\pi^+} = (1.28 \pm 0.03)\text{mb} \qquad (4.2.2)$$

The error is statistical.

4.2.3 CROSS SECTION OF THE REACTION $K^- + p \rightarrow K^- + \pi^- + \Delta^{++}(1236)$

Independent of this study, a fit to the mass spectra of reaction 4.1.2 has been performed using the fit program MAVE2CD[4.15]. The amount of the reaction 4.1.1 was found to be (31 ± 2)% of the reaction 4.1.2. This leads to a cross section

$$\sigma_{K^-p \rightarrow K^-\pi^-\Delta^{++}(1236)} = (0.40 \pm 0.02)\text{mb} \qquad (4.2.3)$$

The contribution of other reaction channels is mentioned in section 4.5.2.

4.2.4 SAMPLE FOR THE ANALYSIS

In order to extract events of reaction 4.1.2 of which the $p\pi^+$ effective mass lies in the $\Delta^{++}(1236)$ region, the following cut is made in the $p\pi^+$ effective mass spectrum:

$$1.14 < m_{p\pi^+} < 1.36 \text{ GeV/c}^2 \qquad (4.2.4)$$

This condition reduces the original sample of 11,046 events to a sample of 4635 events. The cut in the $m_{p\pi^+}$ spectrum is indicated in figure 4.2.2.
The $K^-\pi^-$ Chew Low plot for events which obey this mass cut is given in figure 4.2.3. The figure shows a strong accumulation of events at low four-momentum transfer from the initial K^- meson to the final $K^-\pi^-$ system. This suggests a description of reaction 4.1.1 in terms of a one-meson-exchange mechanism at low four-momentum transfer.

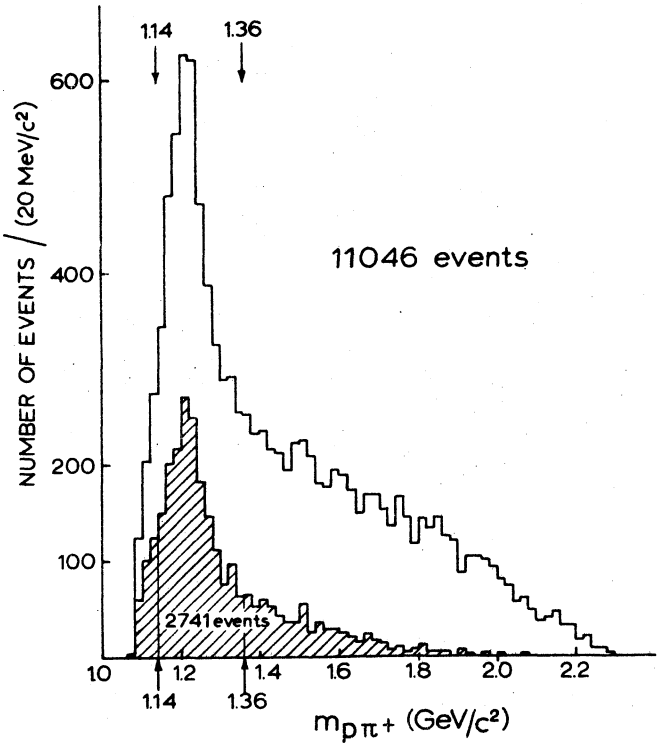

Figure 4.2.2 The $p\pi^+$ effective mass distribution in the reaction $K^- + p \rightarrow K^- + \pi^- + p + \pi^+$. The shaded distribution contains the events with $-t_{K^- \rightarrow K^-\pi^-} < 0.4$ $(GeV/c)^2$: 2741 events. If also $1.14 < m_{p\pi^+} < 1.36$ GeV/c^2: 1758 events.

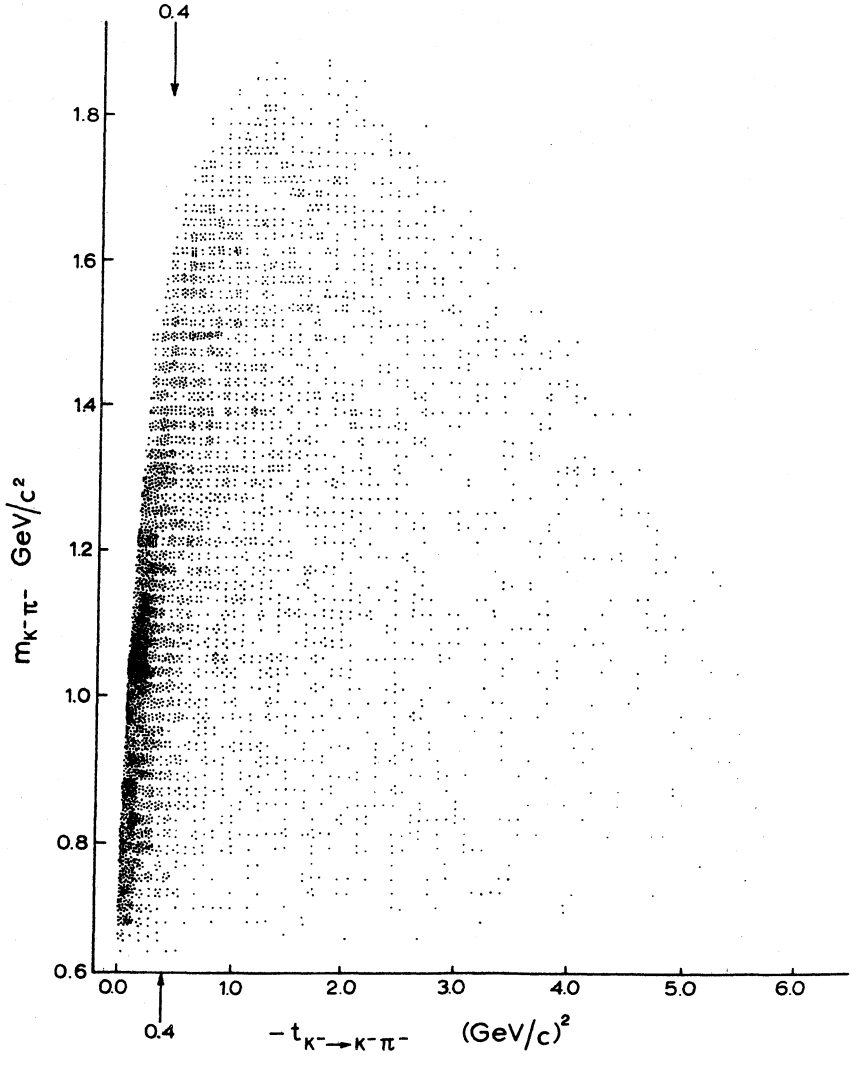

Figure 4.2.3 The $K^-\pi^-$ Chew Low plot for events of the reaction $K^- + p \rightarrow K^- + \pi^- + p + \pi^+$ obeying the condition $1.14 < m_{p\pi^+} < 1.36$ GeV/c^2

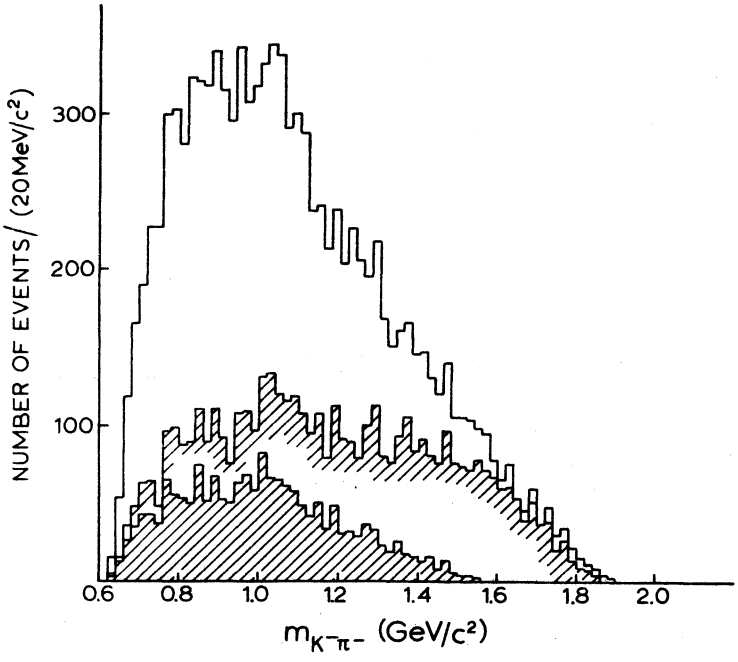

Figure 4.2.4 The $K^-\pi^-$ effective mass distribution in the reaction $K^- + p \rightarrow K^- + \pi^- + p + \pi^+$ for

a. the total sample of 11,046 events (unshaded);

b. the sample of 4635 events which obey the condition 4.2.4 (partially shaded);

c. the sample of 1758 events which obey the conditions 4.2.4 and 4.2.5 (shaded).

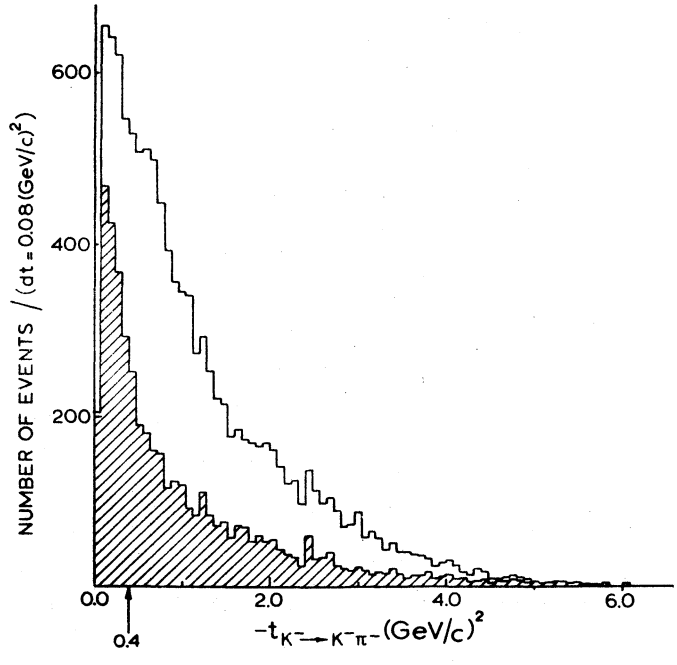

Figure 4.2.5 The distribution of the four-momentum transfer squared in the reaction $K^- + p \rightarrow K^- + \pi^- + p + \pi^+$ for

a. the total sample of 11,046 events (unshaded);

b. the sample of 4635 events which obey the condition 4.2.4 (shaded).

Therefore the analysis has also been restricted to events with

$$- t_{K^- \rightarrow K^-\pi^-} < 0.4 \ (\mathrm{GeV/c})^2 \qquad (4.2.5)$$

The influence of the conditions 4.2.4 and 4.2.5 on the $K^-\pi^-$ effective mass spectrum and the distribution of the four-momentum transfer squared is shown in the figures 4.2.4 and 4.2.5.

The spectrum of the $p\pi^+$ effective mass, for the events satisfying the t-cut, is also shown in figure 4.2.2. As can be expected, these events are restricted mainly to the low effective mass region of the $p\pi^+$ spectrum, and thereby to

the region of the $\Delta^{++}(1236)$ resonance.

Together with the cut on the $p\pi^+$ effective mass (4.2.4) the cut on the four-momentum transfer (4.2.5) reduces the sample which has been used for the analyses of the $K^-\pi^- \to K^-\pi^-$ scattering to 1758 events, containing 1466 unique fits (83.4%) and 292 ambiguous fits (16.6%). The choice of the sample of ambiguous events does not influence the result of the analysis.

4.3 DETERMINATION OF $\sigma_{K^-\pi^-}$

4.3.1 EXTRAPOLATION FORMULA

The $K^-\pi^-$ elastic cross section is obtained from the reaction 4.1.1 with an extrapolation method which was first suggested by G.F. Chew and F.E. Low[4.8]. They considered the virtual pions emitted and re-absorbed by nucleons as loosely bound targets, and based their method on the existence of poles in the scattering matrix implied by such a picture.

In our case, the reaction amplitude R_T for reaction 4.1.1 has a first order pole in the four-momentum transfer at $t_{K^- \to K^-\pi^-} = \mu^2$, where μ is the pion mass ($\hbar = c = 1$).

Furthermore, the residue of the reaction amplitude at the pole can be factorized, i.e. it can be written as the product of the amplitude of the elastic $K^-\pi^-$ scattering $A_{K^-\pi^-}$, and the amplitude of the elastic $p\pi^+$ scattering $B_{p\pi^+}$. The basic hypothesis of analyticity implies that there exists a region in the complex t-plane, including the pole $t = \mu^2$ and the physical part of the real t-axis, in which the Laurent series

$$R_T = \frac{A_{K^-\pi^-}\, B_{p\pi^+}}{t-\mu^2} + \sum_{n=0}^{\infty} \alpha_n (t-\mu^2)^n \qquad (4.3.1)$$

is convergent for any t ($t \neq \mu^2$).

With this series one can derive the formula:

$$C(k^2,s)\, \frac{(t-\mu^2)^2}{\phi(t,m,M)}\, \frac{\partial^3 \sigma_T(s)}{\partial m^2 \partial M^2 \partial t} = \sigma_{K^-\pi^-}(m)\; \sigma_{p\pi^+}(M) + \sum_{n=1}^{\infty} A_n(m,M)(t-\mu^2)^n \qquad (4.3.2)$$

where

$C(k^2,s) = 24.92\, \pi^3 k^2 s$, which is a constant depending on the experiment at hand;

k is the momentum of the incoming K^- meson in the centre of mass system;

s is the square of the total energy in the centre of mass system, $\sqrt{s} = 3.022$ GeV;

$t = t_{K^- \to K^-\pi^-}$ is the square of the four-momentum transfer from the K^- meson to the $K^-\pi^-$ system;

$\sigma_T(s)$ is the total cross section for the reaction $K^- + p \to K^- + \pi^- + p + \pi^+$ depending on the square of the total centre of mass energy of the system, $\sigma_T(3.022) = (1.28 \pm 0.03)$mb (sect. 4.2.2);

$m = m_{K^-\pi^-}$ is the effective mass of the final $K^-\pi^-$ system;

$M = m_{p\pi^+}$ is the effective mass of the final $p\pi^+$ system;

$\sigma_{K^-\pi^-}(m)$ is the unknown cross section of the elastic $K^-\pi^-$ scattering, depending on the $K^-\pi^-$ effective mass;

$\sigma_{p\pi^+}(M)$ is the cross section of the elastic $p\pi^+$ scattering, depending on the $p\pi^+$ effective mass;

$A(m,M)$ are the unknown coefficients of the expansion series;

$\phi(t,m,M) = [(t-(M-m_p)^2)(t-(M+m_p)^2)(t-(m-m_{K^-})^2)(t-(m+m_{K^-})^2)]^{\frac{1}{2}}$;

m_p is the mass of the proton;

m_{K^-} is the mass of the K^- meson.

It is the purpose of this analysis to determine $\sigma_{K^-\pi^-}(m)$. The extrapolation procedure consists of fitting the polynomial in $(t - \mu^2)$ on the right hand side of formula 4.3.2 to the experimental data, with $\sigma_{K^-\pi^-}$ and the coefficients A_n as unknown parameters.

The variable $\sigma_{p\pi^+}(M)$ is well known as a function of the $p\pi^+$ effective mass from other experiments[4.16]. The dependence of $\sigma_{p\pi^+}$ on the $p\pi^+$ effective mass obtained by interpolating and smoothing these experimental values has been sketched in figure 4.3.1.

It should be remarked that in formula 4.3.2, ϕ is a function of t, whereas the original theory of Chew and Low leads to a function ϕ in which t is replaced by μ^2, the pion mass squared. The dependence on t is a modification of the original theory, which is based on the assumption that the one-pion-exchange mechanism dominates reaction 4.1.1 at low four-momentum transfer from the initial K^- meson to the final $K^-\pi^-$ system[4.17]. The OPE diagram for reaction 4.1.1 is sketched in figure 4.3.2. The evidence for a dominant OPE is discussed in section 4.5.7.

The function $\phi(t)$ has the disadvantage that it grows like t^2 as $-t$ increases to $+\infty$. This behaviour of $\phi(t)$ does not agree with the decrease of the experimental differential cross section $d\sigma_T/dt$ with increasing $-t$. In order to save the OPE description, usually empirical form factors are introduced

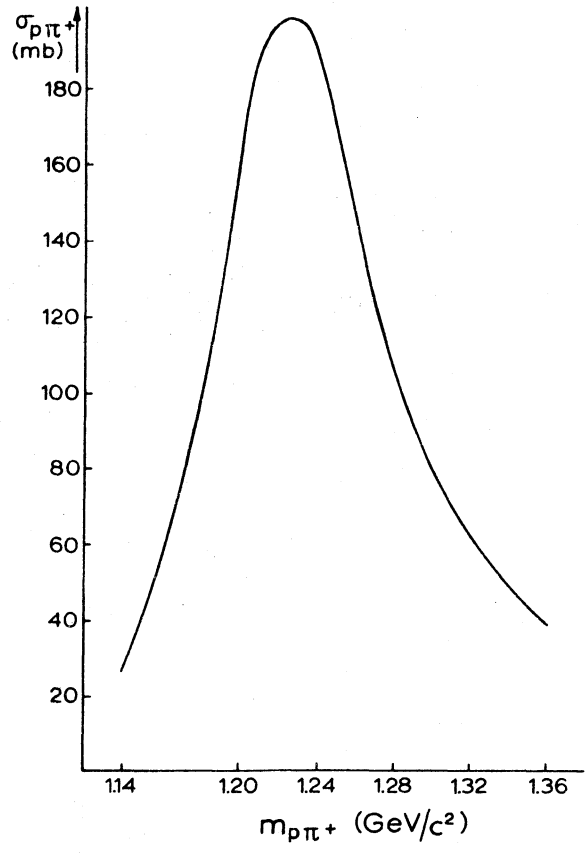

Figure 4.3.1 The cross section of the elastic $\pi^+ p$ scattering $\sigma_{p\pi^+}$, as a function of the $p\pi^+$ effective mass, obtained from reference 4.16

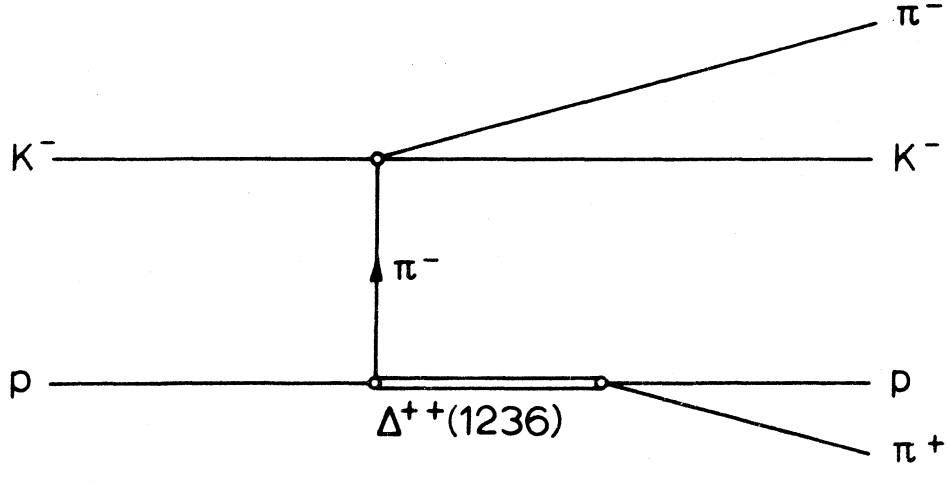

Figure 4.3.2 The one-pion-exchange diagram for the reaction $K^- + p \rightarrow K^- + \pi^- + \Delta^{++}(1236)$

(Dürr-Pilkuhn, Wolf, Benecke-Dürr[4.18]).

Several experiments showed that the OPE model modified with these form factors gives a rather good description of the experimental data[4.19].

In this study no explicite form factors were involved. With only the modification mentioned above, the original theory of Chew and Low will be applied in this work. This seems justified a postiori. In section 4.3.4 the behaviour of the experimental differential cross section $d\sigma_T/dt$ (fig. 4.3.5) is shown to be rather well described by the formula used (the order N of the series being 2).

4.3.2 MAXIMUM LIKELIHOOD METHOD

The determination of $\sigma_{K^-\pi^-}$ as a function of $m_{K^-\pi^-}$ from formula 4.3.2 is made using a maximum likelihood method, as described by D. Linglin[4.20]. In the following sections a short description of this method is given.

4.3.2.1 PROBABILITY FUNCTION. If the series is broken off after the N^{th} term, formula 4.3.2 can be written as

$$\frac{\partial^3\sigma_T}{\partial m^2\partial M^2\partial t} = \frac{\phi}{C(t-\mu^2)^2}\left[\sigma_{K^-\pi^-}\sigma_{p\pi^+} + \sum_{n=1}^{N} A_n(t-\mu^2)^n\right] \qquad (4.3.3)$$

A probability function $P = P(m^2,M^2,t;\sigma_{K^-\pi^-},\sigma_{p\pi^+},A_n)$ $(n = 1,2,\ldots N)$ is then constructed using the right-hand side of equation 4.3.3:

$$P = \frac{1}{N_V\sigma_o}\frac{\phi}{C(t-\mu^2)^2}\left[\sigma_{K^-\pi^-}\sigma_{p\pi^+} + \sum_{n=1}^{N} A_n(t-\mu^2)^n\right] \qquad (4.3.4)$$

The factor $1/N_V\sigma_o$ is due to the normalization of the function P, as described in section 4.3.2.2.

4.3.2.2 NORMALIZATION. The probability function must be normalized, so that

$$\int_V P(m^2,M^2,t)dm^2dM^2dt = 1 \qquad (4.3.5)$$

where V is the physical volume in the (m^2,M^2,t)-space in which $\sigma_{K^-\pi^-}$ will be determined. This is done by normalizing the differential cross section 4.3.3 to the number of events N_V of reaction 4.1.2 in the volume V. Thus

$$\frac{1}{C}\left(\int_V \sigma_{K^-\pi^-}\sigma_{p\pi^+}\frac{\phi}{(t-\mu^2)^2}dV + \sum_{n=1}^{N}\int_V A_n\frac{\phi}{(t-\mu^2)^2}(t-\mu^2)^n dV\right) = N_V\sigma_o \qquad (4.3.6)$$

where $dV = dm^2 dM^2 dt$, and $\sigma_o = \sigma_T/N$ is the cross section per event for the reaction (4.1.2).
With σ_T = (1.28 ± 0.03)mb, determined in section 4.2.2, and the number of events analysed N = 11,046: σ_o = (0.116 ± 0.003)μb/event.

4.3.2.3 CALCULATION OF THE INTEGRALS. The limits of the integration volume are defined by the $K^-\pi^-$ effective mass region for which $\sigma_{K^-\pi^-}$ is to be determined, the $p\pi^+$ effective mass region $1.14 < m_{p\pi^+} < 1.36$ GeV/c^2 and the region of low four-momentum transfer defined by $|t|_{min} < |t| < 0.40$ (GeV/c)^2, where $|t|_{min} = |t|_{min}(m^2_{K^-\pi^-}, m^2_{p\pi^+})$ is the lower limit in the physical region:

$$|t|_{min} = \left[\left\{ \frac{(s+m^2_{p\pi^+}-m^2_{K^-\pi^-})^2}{4s} - m^2_{p\pi^+} \right\}^{\frac{1}{2}} - \left\{ \frac{(s+m^2_p-m^2_{K^-})^2}{4s} - m^2_p \right\}^{\frac{1}{2}}\right]^2 + - \frac{(m^2_{p\pi^+}-m^2_p-m^2_{K^-\pi^-}+m^2_{K^-})^2}{4s} \qquad (4.3.7)$$

where $\sqrt{s}$ is the total energy in the centre of mass system.
Within such an integration volume, the parameters $\sigma_{K^-\pi^-}$ and the A_n are assumed to be constant. No attempt is made to include in the fit a dependence of the parameters on the $K^-\pi^-$ and the $p\pi^+$ effective masses (sect. 4.3.6). Hence, relation 4.3.6 will be written as:

$$\frac{1}{C}\left(\sigma_{K^-\pi^-} \int_V \sigma_{p\pi^+} \frac{\phi}{(t-\mu^2)^2} dV + \sum_{n=1}^{N} A_n \int_V \frac{\phi}{(t-\mu^2)^2}(t-\mu^2)^n dV\right) = N_V \sigma_o \qquad (4.3.8)$$

For the numerical calculations of the integrals in this formula, the two-dimensional ($m_{K^-\pi^-}$, $m_{p\pi^+}$)-area is divided into small sub-areas of about 2 x 2 (MeV/c^2)^2. In the center of these sub-areas $|t|_{min}$ is calculated from relation 4.3.7, and $\sigma_{p\pi^+}$ is obtained by interpolation of the smoothed values of reference 4.16 (fig. 4.3.1). Using these values of $|t|_{min}$ and $\sigma_{p\pi^+}$ the integrals are calculated over each of the corresponding sub-volumes using the Simpson integration formula. The integrals over the whole volume are the sum of the relevant sub-integrals.

4.3.2.4 LIKELIHOOD FUNCTION. The likelihood function for a sample of events confined in a volume V of the (m^2,M^2,t)-space, constructed from the probabilities $P_{V,k}$ per event is

$$L_V = \prod_k P_{V,k} \qquad \text{and} \qquad \ell_V = \log L_V \tag{4.3.9}$$

where k numbers the events per region. For the sake of convenience, the volume index V has been dropped in the following formulas.
For each event, the experimentally determined values of the four-momentum transfer squared $t = t_{K^-\to K^-\pi^-}$ and the $K^-\pi^-$ and $p\pi^+$ effective masses are used to evaluate P_k of formula 4.3.4, which in turn is introduced in formula 4.3.9. The required elastic cross section $\sigma_{p\pi^+}$ is interpolated between the smoothed values of reference 4.16 (fig. 4.3.1).
Maximizing of the likelihood function is a standard iteration procedure. The first and second derivatives $\frac{\partial \ell}{\partial A_n}$, $\frac{\partial^2 \ell}{\partial A_n \partial A_m}$ (n,m = 0,1,....N), with $A_o = \sigma_{K^-\pi^-}$, are calculated using starting values for A_n. In order to determine the A_n, the standard condition is

$$\frac{\partial \ell}{\partial A_n} = 0 \quad (n = 1,....N) \tag{4.3.10}$$

To realize this, the A_n are corrected with dA_n calculated from the N linear equations:

$$\sum_{n=0}^{N} \frac{\partial^2 \ell}{\partial A_m \partial A_n} dA_n = \frac{\partial \ell}{\partial A_m} \quad (m = 0,1....N) \tag{4.3.11}$$

The iteration procedure is repeated until the sum of the first derivatives is smaller than a preset small value.

4.3.2.5 PROCEDURE OF THE CALCULATIONS. The calculations just described are done in several stages. In the first stage the expansion series is cut off after the second term, so that

$$P_k = \frac{1}{N_V \sigma_o C} \frac{\phi_k}{(t_k-\mu^2)^2} (\sigma_{K^-\pi^-} - \sigma^{(k)}_{p\pi^+} + A_1 (t_k-\mu^2)) \tag{4.3.12}$$

The normalization condition becomes

$$\sigma_{K^-\pi^-} \int_V \sigma_{p\pi^+} \frac{\phi}{(t-\mu^2)^2} dV + A_1 \int_V \frac{\phi}{t-\mu^2} dV = N_V \sigma_o C \tag{4.3.13}$$

From this relation one calculates

$$A_1 = \frac{N_V \sigma_o C - \sigma_{K^-\pi^-} \int_V \sigma_{p\pi^+} \frac{\phi}{(t-\mu^2)^2}\, dV}{\int_V \frac{\phi}{t-\mu^2}\, dV} \qquad (4.3.14)$$

Substituting A_1 from relation 4.3.14 into relation 4.3.12 gives

$$P_k = \frac{1}{N_V \sigma_o C} \frac{\phi_k}{(t_k-\mu^2)^2} \left[\sigma_{K^-\pi^-} \left\{ \sigma^{(k)}_{p\pi^+} - \frac{\int_V \sigma_{p\pi^+} \frac{\phi}{(t-\mu^2)^2}\, dV}{\int_V \frac{\phi}{t-\mu^2}\, dV} (t_k-\mu^2) \right\} + \right.$$

$$\left. + \frac{N_V \sigma_o C (t_k-\mu^2)}{\int_V \frac{\phi}{t-\mu^2}\, dV} \right] \qquad (4.3.15)$$

and

$$\ell = \sum_k \log \left[\sigma_{K^-\pi^-} \left\{ \sigma^{(k)}_{p\pi^+} - \frac{\int_V \sigma_{p\pi^+} \frac{\phi}{(t-\mu^2)^2}\, dV}{\int_V \frac{\phi}{t-\mu^2}\, dV} (t_k-\mu^2) \right\} + \right.$$

$$\left. + \frac{N_V \sigma_o C (t_k-\mu^2)}{\int_V \frac{\phi}{t-\mu^2}\, dV} \right] + \sum_k \log \frac{\phi_k}{N_V \sigma_o C (t_k-\mu^2)^2} \qquad (4.3.16)$$

The second series is independent of the parameter $\sigma_{K^-\pi^-}$ and may be omitted in the calculations. For the only parameter $\sigma_{K^-\pi^-}$ a starting value is fixed. Maximizing ℓ with the iteration procedure mentioned gives a result for $\sigma_{K^-\pi^-}$. Using this value, A_1 is calculated from relation 4.3.14.

These two parameters $\sigma_{K^-\pi^-}$ and A_1 determined in the first stage, are used as starting values for the second stage in which one term is added to the expansion series. In the same manner A_2 is eliminated, using the normalization condition. Maximizing the new likelihood function gives results for $\sigma_{K^-\pi^-}$ and A_1, whereas A_2 can be calculated from the normalization condition. The values for $\sigma_{K^-\pi^-}$, A_1 and A_2 determined in this stage, are used as starting values for the third stage, and so on.

A total of four stages have been tried. The calculations have been done with the program EXTRAPOL which is a slightly modified version of the program EXTRAPO[4.20].

4.3.3 RESULTS

For different $K^-\pi^-$ effective mass regions, $\sigma_{K^-\pi^-}$ is calculated from relation 4.3.3, starting with N = 1, and then going successively up to N = 4. The results are presented in table 4.3.2. All errors are statistical and are derived from the square root of the diagonal elements of the inverse of the matrix of derivatives of ℓ with respect to $\sigma_{K^-\pi^-}$ and the A_n. The likelihood for N = 2 appeared to be slightly better than that for N = 1, whereas higher values of N gave no further improvement.

Table 4.3.2 Results for $\sigma_{K^-\pi^-}$ in millibarns, depending on the $K^-\pi^-$ effective mass and the order N of the series in formula 4.3.3.
The $p\pi^+$ effective mass region is given by $1.14 < m_{p\pi^+} < 1.36$ GeV/c^2.
The extrapolation region is limited by the cut $|t|_{max} = 0.4$ (GeV/c)^2.
The results obtained with N = 2 are final. The errors are statistical.

$m_{K^-\pi^-}$ GeV/c^2	number of events	N = 1	N = 2	N = 3	N = 4
< 0.8	314	2.9 ±0.3	1.8 ±0.4	1.6 ±0.4	1.5 ±0.4
< 0.7	74	1.9 ±0.4	1.2 ±0.5	0.6 ±0.6	0.6 ±0.6
0.7 - 0.8	240	3.6 ±0.4	2.5 ±0.5	2.4 ±0.5	2.2 ±0.6
0.8 - 0.9	296	4.4 ±0.4	3.5 ±0.5	3.5 ±0.5	3.3 ±0.5
0.9 - 1.0	291	3.9 ±0.4	3.4 ±0.5	3.3 ±0.5	3.3 ±0.5
1.0 - 1.1	330	4.3 ±0.4	2.8 ±0.5	2.7 ±0.6	2.8 ±0.6
1.1 - 1.2	218	2.6 ±0.4	1.8 ±0.5	1.6 ±0.5	1.6 ±0.5
1.2 - 1.3	157	2.5 ±0.4	2.3 ±0.4	2.4 ±0.4	2.4 ±0.4
1.3 - 1.4	95	2.7 ±0.5	2.7 ±0.5	2.8 ±0.5	2.8 ±0.5
1.2 - 1.4	252	2.5 ±0.3	2.4 ±0.3	2.5 ±0.3	2.5 ±0.3
1.4 - 1.6	57	2.8 ±0.8	2.7 ±0.8	2.7 ±0.8	2.7 ±0.8

It was verified by taking different starting values for $\sigma_{K^-\pi^-}$, that the procedure always converged to the same maximum of the likelihood function. For the final results of $\sigma_{K^-\pi^-}$, with N = 2, the errors have been re-calculated with the S-function of Bartlett for one parameter[4.21].

$$S(\lambda) = \frac{1}{C}\frac{\partial \ell}{\partial \lambda}\ , \text{ with } C^2 = -\int_{\lambda_{min}}^{\lambda_{max}} \frac{\partial^2 \ell}{\partial \lambda^2} L(\lambda)\,d\lambda \qquad (4.3.17)$$

where the parameter $\lambda = \sigma_{K^-\pi^-}$, and λ_{min} and λ_{max} are the integration limits of the region for which $L(\lambda) \gtrsim 0$. For two $K^-\pi^-$ effective mass regions, the functions $S(\lambda)$ and $\ell(\lambda)$ are shown in figure 4.3.3.

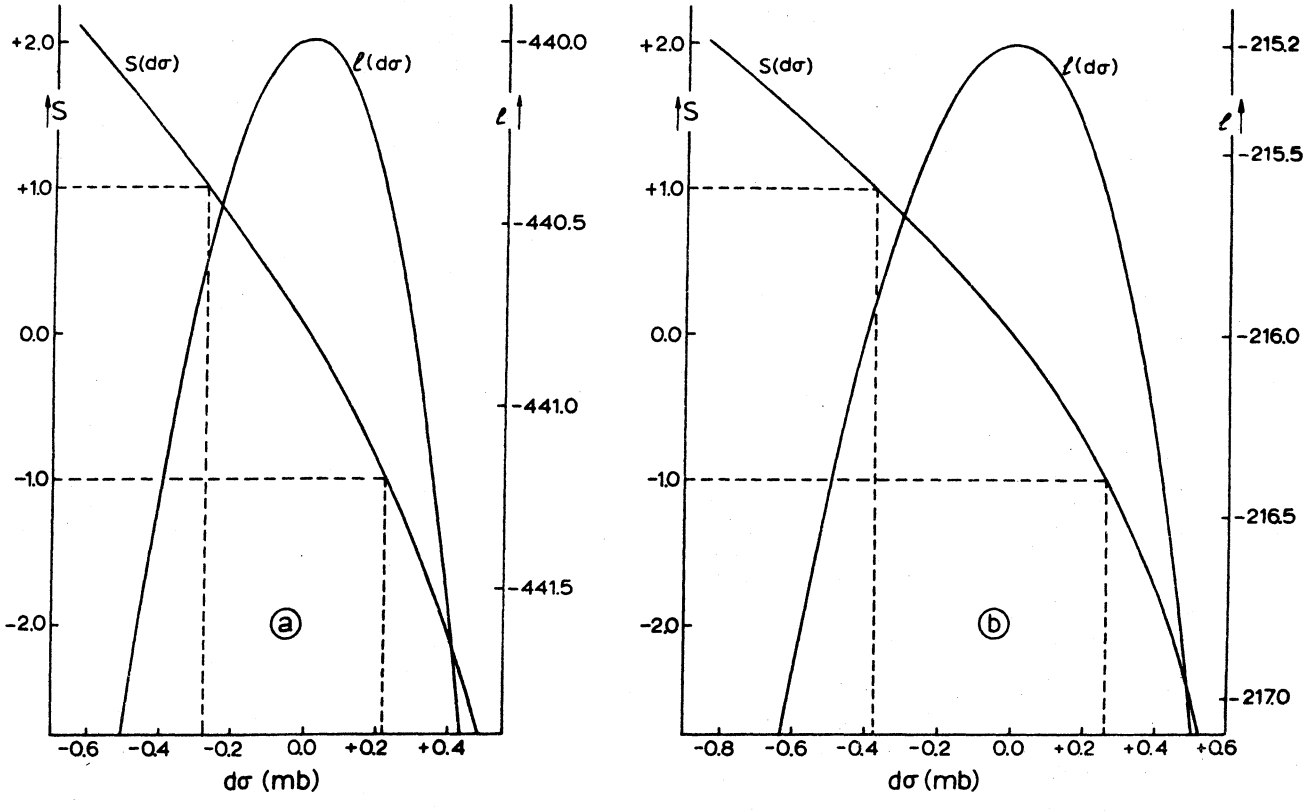

Figure 4.3.3 The S-function of Bartlett and the likelihood function ℓ, depending on the parameter $d\sigma$, for the $K^-\pi^-$ effective mass regions $0.9 < m_{K^-\pi^-} < 1.0$ GeV/c^2(a) and $1.2 < m_{K^-\pi^-} < 1.3$ GeV/c^2(b).
The parameter $d\sigma = \sigma_{K^-\pi^-} - \sigma_{K^-\pi^-}(\ell_{max})$.
The points where $S(d\sigma) = \pm 1$ give the lower and upper error in $\sigma_{K^-\pi^-}$.

The values of $\sigma_{K^-\pi^-}$ for which $S(d\sigma) = \pm 1$, with $d\sigma = \sigma_{K^-\pi^-} - \sigma_{K^-\pi^-(\ell_{max})}$, give the lower and upper errors in $\sigma_{K^-\pi^-}$. These errors, which are shown in table 4.3.3, are somewhat asymmetric. They are somewhat smaller than those obtained from the inverse of the matrix of derivatives.

Table 4.3.3 $\sigma_{K^-\pi^-}$ in millibarns, depending on the $K^-\pi^-$ effective mass. The order N of the series in formula 4.3.3, is 2. The errors are statistical and are obtained using the S-function of Bartlett.

$m_{K^-\pi^-}$ (GeV/c^2)	number of events	$\sigma_{K^-\pi^-}$ (mb)
< 0.7	74	$1.2^{+0.2}_{-0.3}$
0.7 - 0.8	240	$2.5^{+0.2}_{-0.3}$
0.8 - 0.9	296	$3.5^{+0.2}_{-0.3}$
0.9 - 1.0	291	$3.4^{+0.2}_{-0.3}$
1.0 - 1.1	330	$2.8^{+0.2}_{-0.3}$
1.1 - 1.2	218	$1.8^{+0.2}_{-0.3}$
1.2 - 1.3	157	$2.3^{+0.3}_{-0.4}$
1.3 - 1.4	95	$2.7^{+0.5}_{-0.6}$
1.4 - 1.6	57	$2.7^{+0.7}_{-0.9}$

The results for $\sigma_{K^-\pi^-}$ with N = 2, and the errors obtained with the S-function of Bartlett, have been taken as the final results. They have been sketched in figure 4.3.4 as a function of the $K^-\pi^-$ effective mass.

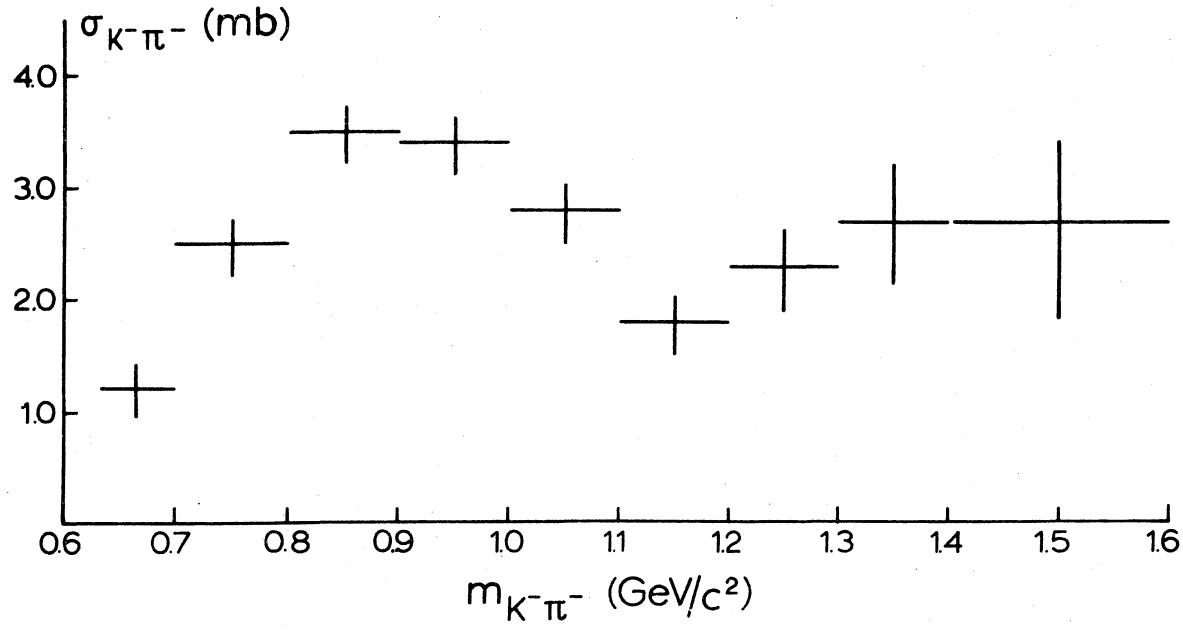

Figure 4.3.4 The elastic cross section $\sigma_{K^-\pi^-}$ in millibarns, depending on the $K^-\pi^-$ effective mass.
The errors are statistical, and are determined with the S-function of Bartlett.

4.3.4 A CHECK ON THE USED PROBABILITY FUNCTION

In order to check the used probability function $P(m^2,M^2,t)$, the distribution of events in the (m,M,t)-space is calculated with this function. - $\sigma_{p\pi^+}$ depends on M; $\sigma_{K^-\pi^-}$ and the A_n are determined as described in the previous sections. - The calculated distribution is compared with the experimental distribution.

Fig. 4.3.5 The distribution of the four-momentum transfer squared $t = t_{K^-\rightarrow K^-\pi^-}$ in the region $-t < 0.4$ $(GeV/c)^2$ for events with a $p\pi^+$ effective mass satisfying $1.14 < m_{p\pi^+} < 1.36$ GeV/c^2, in the different regions of the $K^-\pi^-$ effective mass (in GeV/c^2).
The distributions, which are calculated from the probability function 4.3.4 (with 4.3.18) with the order N of the series 2 and 1, are indicated by an uninterrupted line and a dashed line respectively. The total number of events in a figure are given, together with those calculated for N = 2 and N = 1.

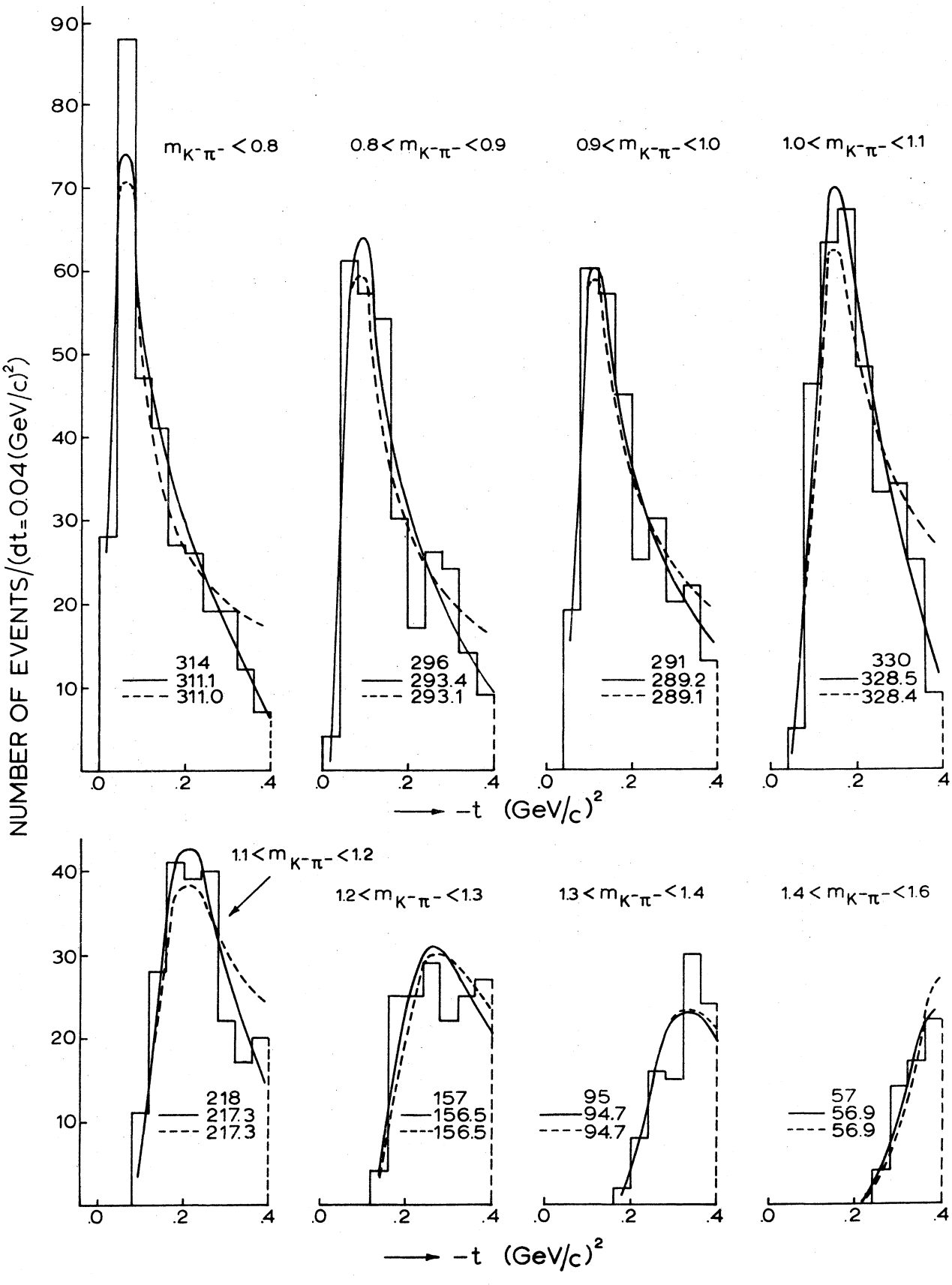
NUMBER OF EVENTS/(dt=0.04(GeV/c)²)
$m_{K^-\pi^-} < 0.8$
$0.8 < m_{K^-\pi^-} < 0.9$
$0.9 < m_{K^-\pi^-} < 1.0$
$1.0 < m_{K^-\pi^-} < 1.1$
314
311.1
311.0
296
293.4
293.1
291
289.2
289.1
330
328.5
328.4
$-t$ (GeV/c)²
$1.1 < m_{K^-\pi^-} < 1.2$
$1.2 < m_{K^-\pi^-} < 1.3$
$1.3 < m_{K^-\pi^-} < 1.4$
$1.4 < m_{K^-\pi^-} < 1.6$
218
217.3
217.3
157
156.5
156.5
95
94.7
94.7
57
56.9
56.9
$-t$ (GeV/c)²

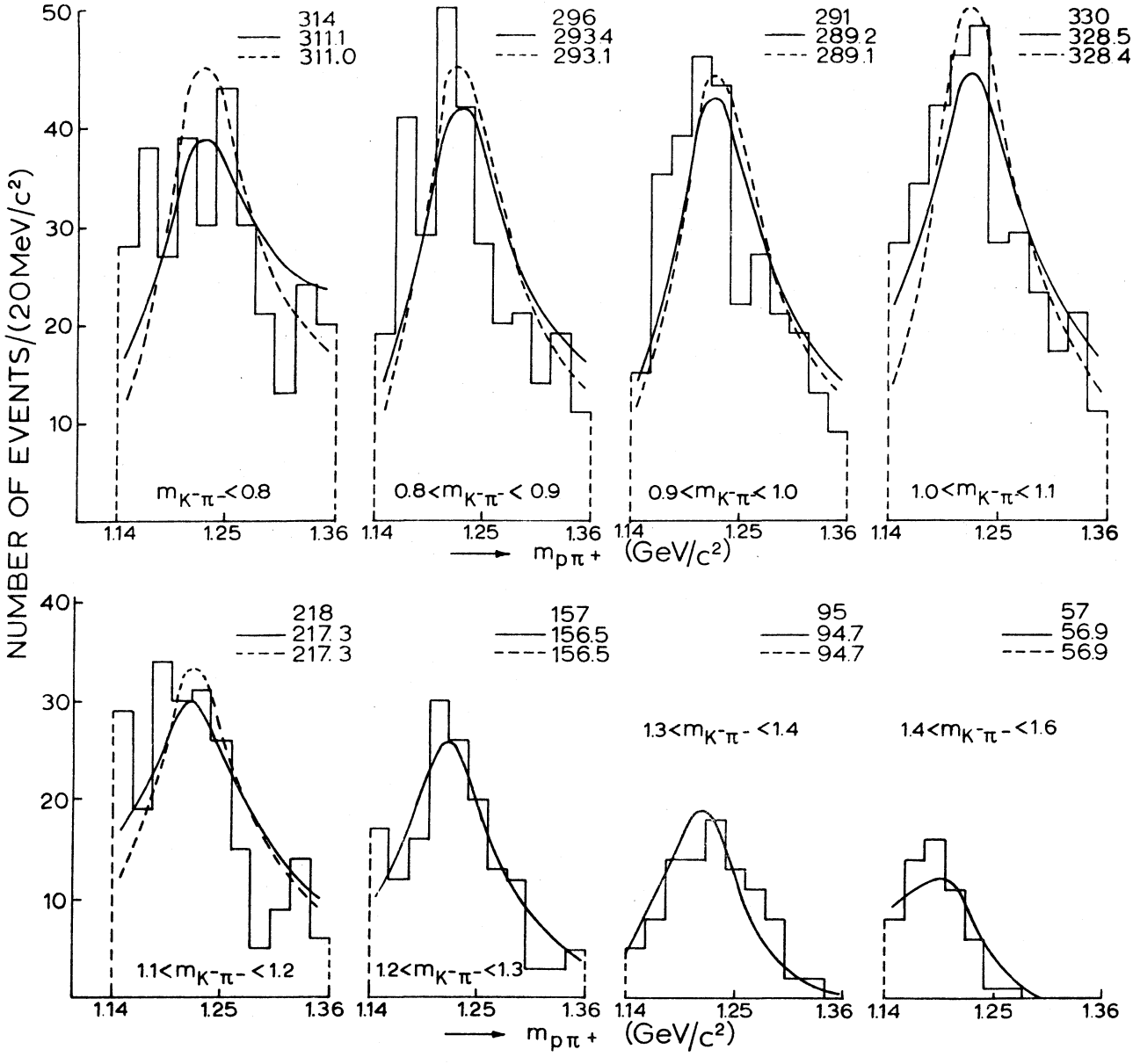

Fig. 4.3.6 The $p\pi^+$ effective mass distribution in the region $1.14 < m_{p\pi^+} < 1.36$ GeV/c^2 for events with low four-momentum transfer $-t_{K^- \to K^-\pi^-} < 0.4$ (GeV/c)^2, in the different regions of the $K^-\pi^-$ effective mass (in GeV/c^2).

The distributions, which are calculated from the probability function 4.3.4 (with 4.3.18) with the order N of the series 2 and 1, are indicated by an uninterrupted line and a dashed line respectively. For $m_{K^-\pi^-} > 1.2$ GeV/c^2, the curves for N = 1 are not sketched, because they are almost the same as for N = 2. The total number of events in a figure are given, together with those calculated for N = 2 and N = 1.

The distribution function D is obtained from the probability function P by normalizing this function to the number of events N_V in the volume V concerned. For the sake of convenience the variables are changed from m^2, M^2, t into m, M, t. Hence $D(m,M,t) = 4\,mMN_V\,P(m^2,M^2,t)$. The number of events in a volume dV = dmdMdt around a point (m_o,M_o,t_o), with $m_o - 1/2\,dm < m < m_o + 1/2\,dm$, $M_o - 1/2\,dM < M < M_o + 1/2\,dM$, and $t_o - 1/2\,dt < t < t_o + 1/2\,dt$, is given by

$$dN = 4m_oM_oN_V\,P(m^2,M^2,t)\,dmdMdt \qquad (4.3.18)$$

Near the physical limit of t, the volume dV is cut by the surface described by formula 4.3.7. In this volume dV, sub-volumes are constructed by dividing dm and dM in sub-regions of 2 MeV/c^2. Of each sub-volume, the physically possible dt and the centre value of t is calculated. dN is added over the sub-volumes.

Figures 4.3.5 and 4.3.6 show the experimental distributions depending on t and $m_{p\pi^+}$ respectively, for the different $K^-\pi^-$ effective mass regions. In both figures the distributions are also shown calculated from formula 4.3.18, the order N of the series of formula 4.3.4 being 2 and 1. Figure 4.3.5 shows that the t dependence of the experimental data is better described with N = 2 than with N = 1. The curves in figure 4.3.6 are mainly determined by the curve of the experimental elastic $p\pi^+$ scattering cross section of figure 4.3.1, which has been used in formula 4.3.18 in the same way as described in section 4.3.2.3.

4.3.5 SOME REMARKS ON THE CHOICE OF THE SAMPLE OF EVENTS

The choice of the events using the cuts $1.14 < m_{p\pi^+} < 1.36$ GeV/c^2 and $|t| < 0.4$ (GeV/c)^2 might be somewhat arbitrary. To examine the influence of these cuts on the results, the determination of $\sigma_{K^-\pi^-}$ has also been made, using samples with different cuts.

Table 4.3.4 shows the results for different cuts in the spectrum of the $p\pi^+$ effective mass. The results for different mass cuts are compatible with each other. Since the relative amount of the background grows when a broader mass cut is made, this test suggest that the influence of the background on the results is small.

Table 4.3.4 $\sigma_{K^-\pi^-}$ in millibarns, depending on the $K^-\pi^-$ effective mass and the width of the $p\pi^+$ effective mass region around $m_{p\pi^+} = 1.236$ GeV/c^2.

The extrapolation region is given by $|t| < 0.4$ (GeV/c)^2. The order of the series of formula 4.3.3 is 2. N_V is the number of events in the (m,M,t) volume concerned. The errors are statistical.

	$m_{p\pi^+}$ (GeV/c^2)							
	1.14-1.36		1.16-1.335		1.18-1.31		1.20-1.285	
$m_{K^-\pi^-}$ (GeV/c^2)	N_V	$\sigma_{K^-\pi^-}$ (mb)	N_V	$\sigma_{K^-\pi^-}$ (mb)	N_V	$\sigma_{K^-\pi^-}$ (mb)	N_V	$\sigma_{K^-\pi^-}$ (mb)
< 0.8	314	1.8 ±0.4	264	2.1 ±0.4	196	2.4 ±0.6	148	1.6 ±0.8
0.8 - 0.9	296	3.5 ±0.5	261	3.5 ±0.6	199	4.4 ±0.8	150	4.0 ±1.2
0.9 - 1.0	291	3.4 ±0.5	263	3.1 ±0.7	210	3.2 ±0.8	144	3.1 ±1.2
1.0 - 1.1	330	2.8 ±0.5	287	2.8 ±0.7	229	2.7 ±0.9	159	3.0 ±1.3
1.1 - 1.2	218	1.8 ±0.5	179	2.7 ±0.6	144	3.7 ±0.8	104	2.5 ±1.2
1.2 - 1.4	252	2.4 ±0.3	224	3.3 ±0.4	197	3.7 ±0.7	152	2.8 ±1.1

Table 4.3.5 shows the results for different cuts in the spectrum of the four-momentum transfer squared $t = t_{K^- \to K^-\pi^-}$. Again the differences are not significant and the results are equal within the errors. Since these results do not differ systematically, the cut $-t < 0.4$ (GeV/c)^2 is chosen in order to enlarge the statistics. - In the tables 4.3.4 and 4.3.5 the errors are obtained from the inverse of the matrix of derivatives. -

Table 4.3.5 $\sigma_{K^-\pi^-}$ in millibarns, depending on the $K^-\pi^-$ effective mass and the upper limit of the extrapolation region $|t|_{max}$.
The $p\pi^+$ effective mass region is given by $1.14 < m_{p\pi^+} < 1.36$ GeV/c^2.
The order of the series of formula 4.3.3 is 2. N_V is the number of events in the (m,M,t)-volume concerned. The errors are statistical.

	$\|t\|_{max}$ (GeV/c)^2									
	0.40		0.32		0.24		0.16		0.08	
$m_{K^-\pi^-}$ (GeV/c^2)	N_V	$\sigma_{K^-\pi^-}$ (mb)	N_V	$\sigma_{K^-\pi^-}$ (mb)	N_V	$\sigma_{K^-\pi^-}$ (mb)	N_V	$\sigma_{K^-\pi^-}$ (mb)	N_V	$\sigma_{K^-\pi^-}$ (mb)
< 0.8	314	1.8 ±0.4	295	1.8 ±0.4	257	1.6 ±0.5	204	1.3 ±0.5	116	1.1 ±0.7
0.8-0.9	296	3.5 ±0.5	273	3.7 ±0.5	223	3.1 ±0.6	176	3.6 ±0.8	65	3.3 ±1.5
0.9-1.0	291	3.4 ±0.5	256	3.6 ±0.5	206	3.5 ±0.6	136	3.0 ±0.8		
1.0-1.1	330	2.8 ±0.5	296	3.3 ±0.6	229	3.2 ±0.8	114	2.9 ±1.0		
1.1-1.2	218	1.8 ±0.5	181	2.0 ±0.5	119	2.3 ±0.7	39	2.1 ±1.5		
1.2-1.4	252	2.4 ±0.3	146	2.0 ±0.4	64	2.1 ±0.7				

4.3.6 SOME REMARKS ON THE STRUCTURE OF THE PARAMETERS

As remarked in section 4.3.2.3, no dependence on the $K^-\pi^-$ and $p\pi^+$ effective masses was introduced for the parameters $\sigma_{K^-\pi^-}$ and A_n (n = 1,...4) within an integration volume.

Table 4.3.2 shows that $\sigma_{K^-\pi^-}$ depends at most only slightly on the $K^-\pi^-$ effective mass. It has also been checked, that $\sigma_{K^-\pi^-}$ does not depend appreciably on the $p\pi^+$ effective mass.

The dependence of the coefficients A_n on the $K^-\pi^-$ effective mass is shown in table 4.3.6. The calculations have been done using four terms of the series 4.3.3. With the normalizing condition A_4 is calculated from $\sigma_{K^-\pi^-}$, A_1, A_2 and A_3. The errors in A_n - obtained from the inversed matrix of derivatives - are large, especially in the higher $K^-\pi^-$ effective mass regions, where the errors are of the same order as the values of A_n. The table shows, within this

context, that the A_n do not significantly depend on the $K^-\pi^-$ effective mass. It has also been checked, that the A_n do not depend on the $p\pi^+$ effective mass.

Table 4.3.6 Results for A_n (n = 1,2,3,4) in $(mb)^2/(GeV/c)^{2n}$ depending on the $K^-\pi^-$ effective mass.
The $p\pi^+$ effective mass region is given by $1.14 < m_{p\pi^+} < 1.36$ GeV/c^2. The extrapolation region is limited by the cut $|t|_{max} = 0.4\ (GeV/c)^2$. The order N of the series in formula 4.3.3 is 4. The errors are statistical.

$m_{K^-\pi^-}$ GeV/c^2	number of events	$A_1 \times 10^{-3}$	$A_2 \times 10^{-4}$	$A_3 \times 10^{-5}$	$A_4 \times 10^{-5}$
< 0.8	314	-5.7 ±1.8	-4.2 ±2.3	-1.3 ±1.0	-1.5
< 0.7	74	-4.4 ±2.6	-2.4 ±3.1	-0.4 ±1.3	-0.2
0.7 - 0.8	240	-6.6 ±2.6	-5.8 ±3.3	-2.1 ±1.4	-2.5
0.8 - 0.9	296	-7.3 ±2.8	-7.8 ±3.5	-3.1 ±1.4	-3.9
0.9 - 1.0	291	-4.5 ±3.0	-4.3 ±3.7	-1.6 ±1.4	-1.9
1.0 - 1.1	330	-12.8 ±3.9	-12.1 ±4.5	-4.2 ±1.6	-4.9
1.1 - 1.2	218	-9.0 ±5.1	-6.7 ±5.6	-1.8 ±2.0	-1.6
1.2 - 1.3	157	-3.3 ±8.7	-1.1 ±9.0	+0.3 ±3.0	+0.8
1.3 - 1.4	95	-18.0 ±18.4	-16.7 ±17.4	-5.0 ±5.4	-5.0
1.2 - 1.4	252	-7.9 ±7.2	-6.2 ±7.2	-1.6 ±2.4	-1.2
1.4 - 1.6	57	+38.8 ±92.2	+30.4 ±81.0	+7.6 ±23.5	+6.2

From these results it may be concluded that the use of constant values for $\sigma_{K^-\pi^-}$ and the A_n in the integration volumes, is allowed. - A simular conclusion was made by Linglin[4·20] for the A_n in a determination of the elastic $K^+\pi^-$ cross section $\sigma_{K^+\pi^-}$ from the reaction $K^+ + p \to K^+ + \pi^- + p + \pi^+$. He gave the A_n a dependence on the $K^+\pi^-$ effective mass and did not find a significant influence on the results for $\sigma_{K^+\pi^-}$.

4.4 STUDY OF THE $K^-\pi^-$ SCATTERING ANGULAR DISTRIBUTION

4.4.1 FORMALISM OF THE PARTIAL WAVE EXPANSION

In a further analysis of the $K^-\pi^-$ interaction, the scattering angles of the final K^- meson in the $K^-\pi^-$ rest system have been studied.
The differential cross section for the on-mass-shell elastic $K^-\pi^-$ scattering is extremely simple in the partial wave formalism since no spin is involved and the system is in a pure isopin I = 3/2 state:

$$\frac{d\sigma_{el}}{d\Omega} = \frac{4\pi}{k^2} \left| \sum_{\ell=0}^{\infty} \sqrt{2\ell+1}\, \frac{e^{2i\delta^3_\ell}-1}{2i}\, Y^0_\ell \right|^2 \qquad (4.4.1)$$

In this formula k is the momentum of the K^- meson in the $K^-\pi^-$ center of mass system ($\hbar = c = 1$), ℓ is the orbital angular momentum, Y^0_ℓ are the spherical harmonics and δ^3_ℓ is the I = 3/2 phase shift for the ℓ-wave[4.22].
The total elastic cross section becomes

$$\sigma_{el} = \frac{4\pi}{k^2} \sum_{\ell=0}^{\infty} (2\ell+1)\, \sin^2\delta^3_\ell \qquad (4.4.2)$$

The spherical harmonics Y^0_ℓ form a complete orthonormal set. Normalizing on the total elastic cross section σ_{el}, formula 4.4.1 may be written as

$$\frac{1}{\sigma_{el}} \frac{d\sigma_{el}}{d\Omega} = \sum_{L=0}^{\infty} \langle Y^0_L \rangle\, Y^0_L \qquad (4.4.3)$$

where $\langle Y^0_L \rangle$ (L = 0,1,..∞) are the spherical harmonic moments of the scattering angular distribution.
Assuming that only s- and p-waves contribute to elastic $K^-\pi^-$ scattering, formula 4.4.1 and 4.4.2 can be written as

$$\frac{d\sigma_{el}}{d\Omega} = \frac{4\pi}{k^2} \left[\frac{1}{4\pi} (\sin^2\delta^3_0 + 3\sin^2\delta^3_1) + \sqrt{\frac{3}{\pi}} \sin\delta^3_0 \sin\delta^3_1 \times \right.$$

$$\left. \times \cos(\delta^3_0 - \delta^3_1)\, Y^0_1 + \frac{3}{\sqrt{5\pi}} \sin^2\delta^3_1\, Y^0_2 \right] \qquad (4.4.4)$$

and

$$\sigma_{el} = \frac{4\pi}{k^2} (\sin^2\delta^3_0 + 3\sin^2\delta^3_1) \qquad (4.4.5)$$

With relation 4.4.3:

$$\langle Y_1^0 \rangle = \sqrt{\frac{3}{\pi}} \frac{\sin \delta_0^3 \sin \delta_1^3 \cos(\delta_0^3 - \delta_1^3)}{\sin^2 \delta_0^3 + 3 \sin^2 \delta_1^3} \tag{4.4.6}$$

and

$$\langle Y_2^0 \rangle = \frac{3}{\sqrt{5\pi}} \frac{\sin^2 \delta_1^3}{\sin^2 \delta_0^3 + 3 \sin^2 \delta_1^3} \tag{4.4.7}$$

The on-mass-shell values $\sigma_{K^-\pi^-}$, $\langle Y_1^0 \rangle$ and $\langle Y_2^0 \rangle$ can be obtained from the experimental data by extrapolation to the pion pole. Thus the relations 4.4.5, 4.4.6 and 4.4.7 form a set of three equations with the phase shifts δ_0^3 and δ_1^3 as two unknown variables; A one-constraint fit can be made.

4.4.2 $K^-\pi^-$ SCATTERING ANGLES

The scattering angles θ_K and ϕ_K of the final K^- meson in the Jackson frame in the $K^-_{final}\pi^-$ rest system, which are shown in figure 4.4.1, are defined by

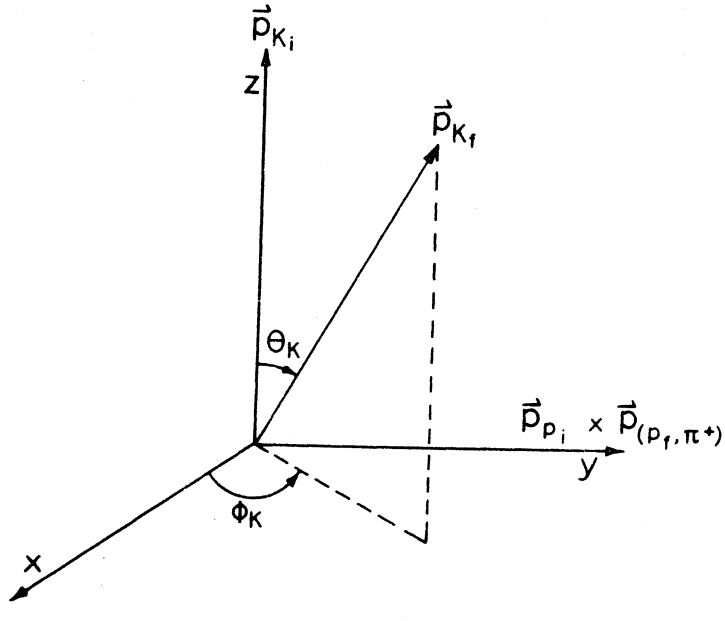

Fig. 4.4.1 The angles θ_K and ϕ_K of the final K^- meson K_f^- in the Jackson frame in the $K^-\pi^-$ rest system.
(x,z) is the production plane.
p_{K_i}, p_{K_f}, p_{p_i} and $p_{(p_f,\pi^+)}$ are respectively the momentum vectors of the incoming K^- meson, the outgoing K^- meson, the incoming

$$\cos\theta_K = \frac{\vec{p}_{K_i} \cdot \vec{p}_{K_f}}{|\vec{p}_{K_i}|\,|\vec{p}_{K_f}|} \qquad (4.4.8.a)$$

$$\phi_K = \arccos \frac{\vec{p}_{p_i} \wedge \vec{p}_{(p_f,\pi^+)}}{|\vec{p}_{p_i} \wedge \vec{p}_{(p_f,\pi^+)}|} \cdot \frac{\vec{p}_{K_i} \wedge \vec{p}_{K_f}}{|\vec{p}_{K_i} \wedge \vec{p}_{K_f}|} \qquad (4.4.8.b)$$

$$\phi_K = \arcsin \frac{\vec{p}_{K_i} \wedge (\vec{p}_{p_i} \wedge \vec{p}_{(p_f,\pi^+)})}{|\vec{p}_{K_i} \wedge (\vec{p}_{p_i} \wedge \vec{p}_{(p_f,\pi^+)})|} \cdot \frac{\vec{p}_{K_i} \wedge \vec{p}_{K_f}}{|\vec{p}_{K_i} \wedge \vec{p}_{K_f}|} \qquad (4.4.8.c)$$

$\vec{p}_{K_i}$ is the momentum vector of the incoming K^- meson,

$\vec{p}_{K_f}$ is the momentum vector of the outgoing K^- meson,

$\vec{p}_{p_i}$ is the momentum vector of the incoming proton,

$\vec{p}_{(p_f,\pi^+)}$ is the momentum vector of the outgoing $p\pi^+$ system, all defined in the $K^-_{final}\pi^-$ rest system.

For events which obey the conditions for the $p\pi^+$ effective mass 4.2.4 and the four-momentum transfer squared $t_{K^- \to K^-\pi^-}$ 4.2.5, the distribution of $\cos\theta_K$ and ϕ_K are shown in figure 4.4.2.

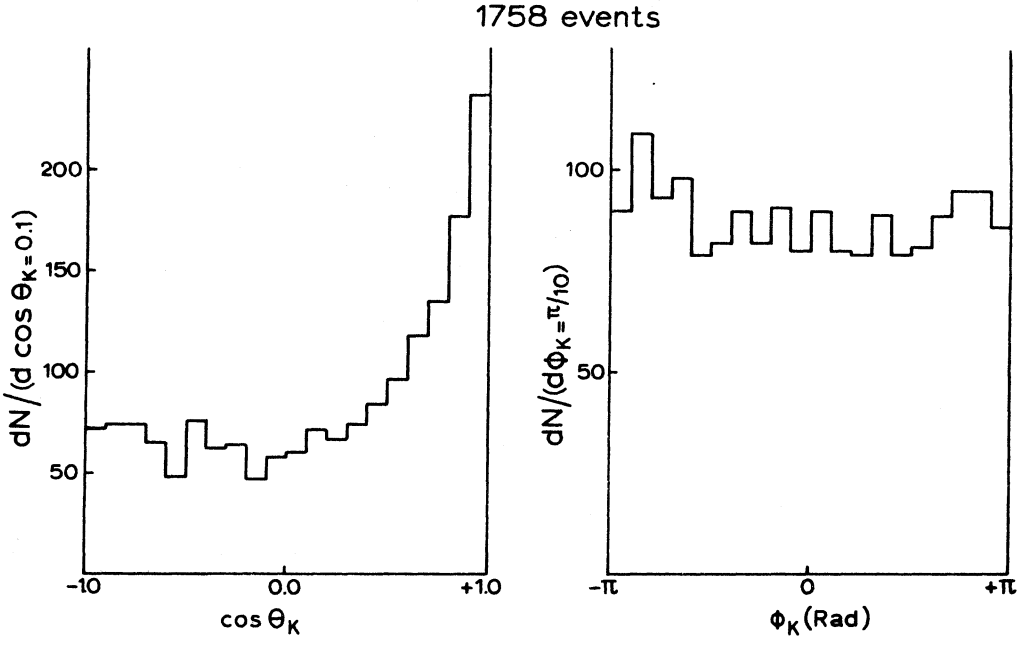

Figure 4.4.2 The $\cos\theta_K$ and ϕ_K distributions for events of the reaction $K^- + p \to K^- + \pi^- + p + \pi^+$ that obey the conditions $1.14 < m_{p\pi^+} < 1.36$ GeV/c^2 and $-t_{K^- \to K^-\pi^-} < 0.4$ (GeV/c)^2

Figure 4.4.3 shows the variation of the cos θ_K distribution with increasing $K^-\pi^-$ effective mass. From this figure it can be seen that the asymmetry in cos θ_K is very small for the lower $K^-\pi^-$ effective mass regions, whereas it becomes pronounced for the higher $K^-\pi^-$ effective mass regions.

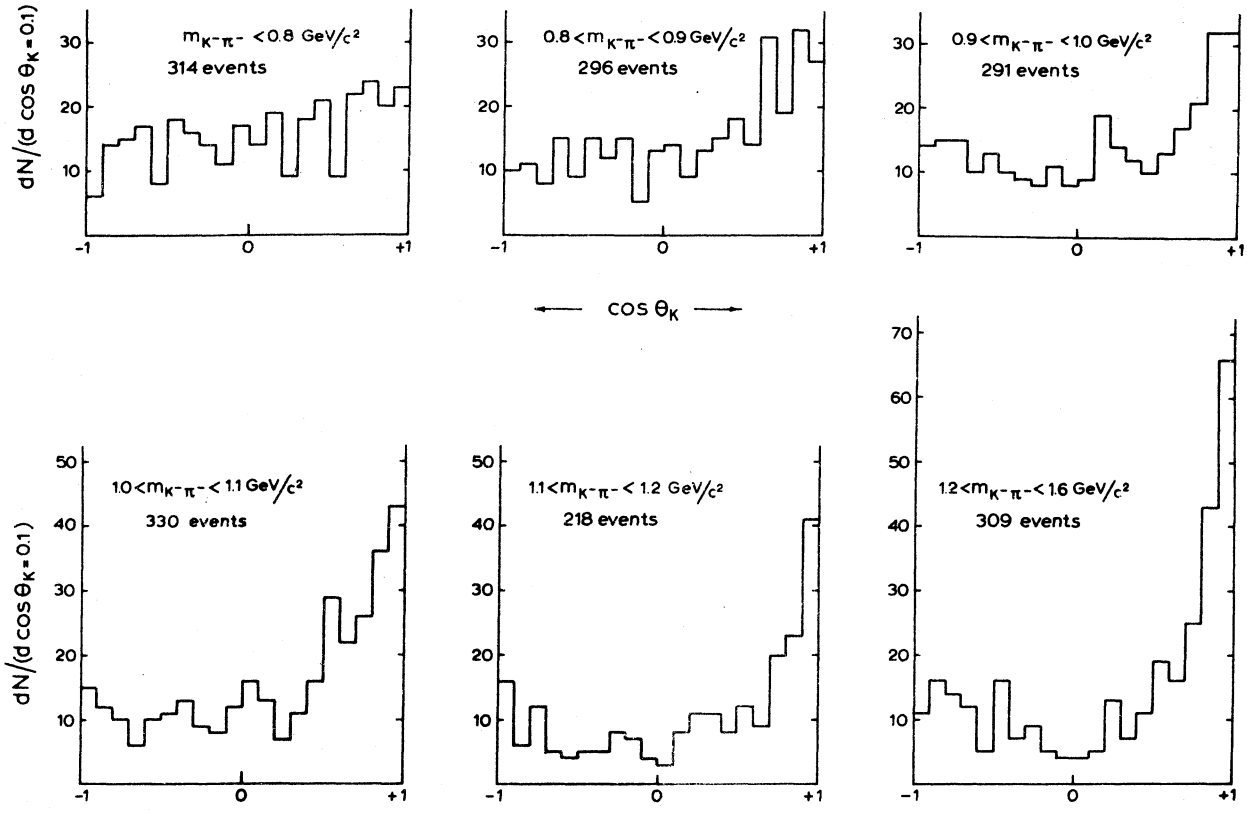

Figure 4.4.3 The variation of the cos θ_K distribution with increasing $K^-\pi^-$ effective mass

4.4.3 OFF-MASS-SHELL MOMENTS

The dependence of the off-mass-shell moments of some of the spherical harmonics on the $K^-\pi^-$ effective mass is shown in table 4.4.1 and in the figure 4.4.4 and 4.4.5. These moments have been averaged over the four-momentum transfer region $(-t)_{min} < -t_{K^- \to K^-\pi^-} < 0.4$ $(GeV/c)^2$, and the region of the $p\pi^+$ effective mass $1.14 < m_{p\pi^+} < 1.36$ GeV/c^2. The errors are statistical. From figure 4.4.4 it can be seen that the lower the $K^-\pi^-$ effective mass, the smaller $\langle Y_1^0 \rangle$ and $\langle Y_2^0 \rangle$ become. The higher moments with m = 0 are compatible with zero for the lower $K^-\pi^-$ effective mass regions. At $m_{K^-\pi^-} \approx 1.1$ GeV/c^2, they deviate significantly from zero and become positive. In an analysis of the $K^-\pi^-$ scattering in the reaction $K^- + n \to K^- + \pi^- + p$ at 3 GeV/c incident K^- momentum, Bakker[4.23] found an analogous behaviour for the moments $\langle Y_1^0 \rangle$ through $\langle Y_4^0 \rangle$ for $m_{K^-\pi^-} < 1.2$ GeV/c^2. When drawing attention to the bump in

Table 4.4.1 Off-mass-shell moments as a function of the $K^-\pi^-$ effective mass.

The moments are determined from events of the reaction $K^- + p \to K^- + \pi^- + p + \pi^+$ that obey the conditions $1.14 < m_{p\pi^+} < 1.36$ GeV/c^2 and $-t_{K^- \to K^-\pi^-} < 0.4$ (GeV/c)^2. They have been avaraged over these regions.

$m_{K^-\pi^-}$ (GeV/c^2)	number of events	$\langle Y_1^0 \rangle$	$\langle Y_2^0 \rangle$	$\langle Y_3^0 \rangle$	$\langle Y_4^0 \rangle$	$\langle Y_5^0 \rangle$	$\langle Y_6^0 \rangle$	$\langle Y_7^0 \rangle$	$\langle Y_8^0 \rangle$	$\langle \mathrm{Re}Y_1^1 \rangle$	$\langle \mathrm{Re}Y_2^1 \rangle$	$\langle \mathrm{Re}Y_2^2$
< 0.8	314	0.054 ±0.016	0.013 ±0.016	0.021 ±0.016	-0.014 ±0.016	-0.006 ±0.017	-0.015 ±0.017	-0.007 ±0.016	0.028 ±0.017	0.045 ±0.011	-0.010 ±0.012	0.016 ±0.0
0.8-0.9	296	0.083 ±0.017	0.040 ±0.017	0.011 ±0.017	-0.017 ±0.017	-0.012 ±0.017	0.009 ±0.017	-0.001 ±0.017	0.015 ±0.017	0.020 ±0.011	-0.011 ±0.012	0.000 ±0.0
0.9-1.0	291	0.075 ±0.018	0.089 ±0.018	0.028 ±0.018	0.018 ±0.018	0.015 ±0.018	-0.022 ±0.018	-0.012 ±0.018	0.021 ±0.018	0.015 ±0.011	-0.023 ±0.012	0.006 ±0.0
1.0-1.1	330	0.130 ±0.016	0.105 ±0.017	0.047 ±0.018	0.042 ±0.019	0.028 ±0.018	0.037 ±0.019	0.057 ±0.019	0.047 ±0.019	-0.017 ±0.010	0.000 ±0.011	-0.005 ±0.0
1.1-1.2	218	0.126 ±0.022	0.157 ±0.022	0.050 ±0.024	0.080 ±0.024	0.042 ±0.025	0.054 ±0.024	0.028 ±0.024	0.047 ±0.024	0.005 ±0.011	0.028 ±0.013	-0.011 ±0.0
1.2-1.3	157	0.113 ±0.026	0.148 ±0.023	0.104 ±0.025	0.006 ±0.025	0.049 ±0.026	0.008 ±0.025	0.002 ±0.025	-0.009 ±0.024	-0.011 ±0.013	-0.033 ±0.017	-0.012 ±0.0
1.3-1.4	95	0.181 ±0.031	0.175 ±0.030	0.097 ±0.033	0.015 ±0.035	0.001 ±0.034	0.001 ±0.033	0.029 ±0.033	0.042 ±0.033	-0.008 ±0.017	-0.036 ±0.022	-0.010 ±0.0
1.4-1.6	57	0.186 ±0.047	0.330 ±0.038	0.111 ±0.058	0.218 ±0.052	0.121 ±0.058	0.160 ±0.058	0.075 ±0.061	0.107 ±0.063	0.013 ±0.017	-0.005 ±0.026	-0.017 ±0.0

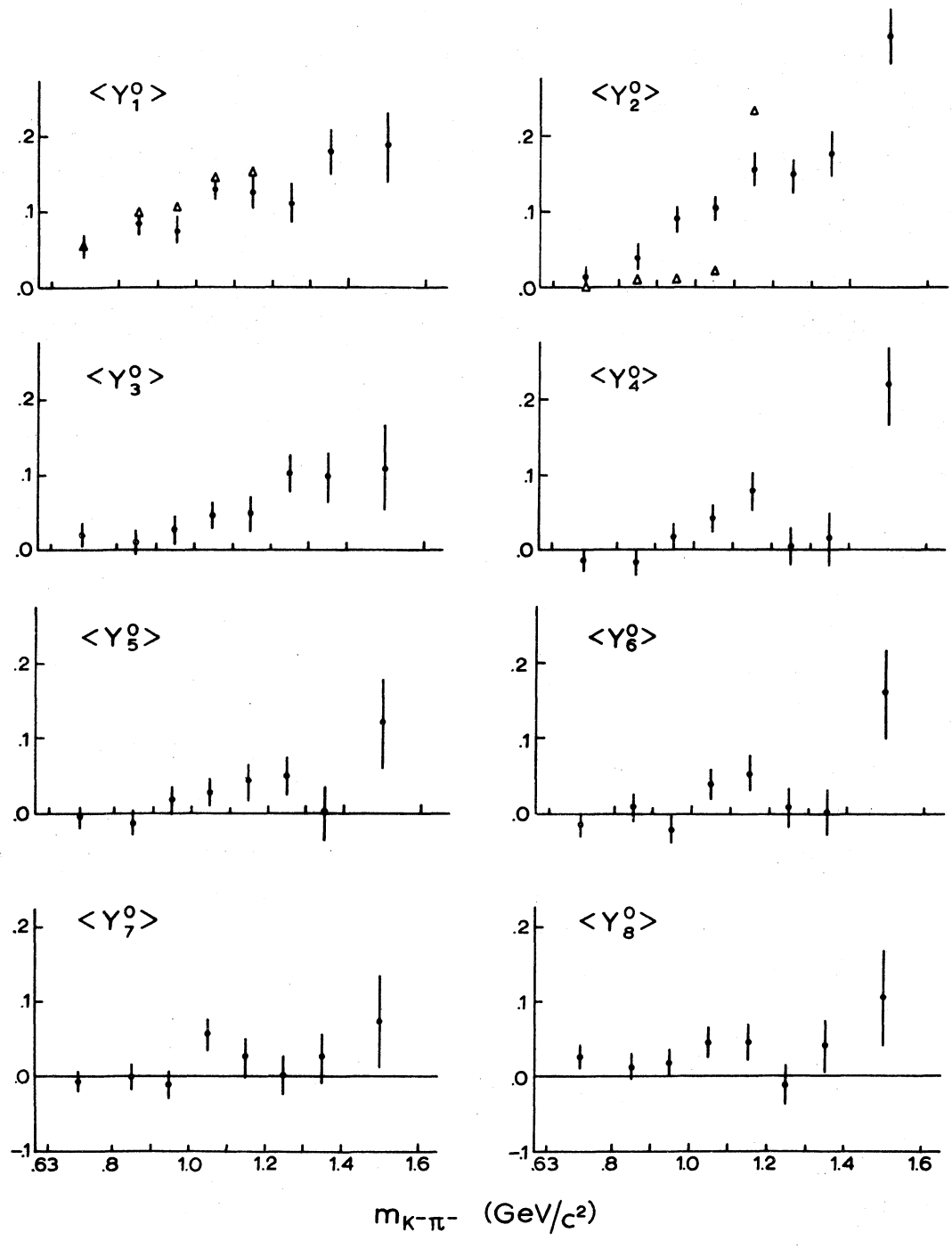

Fig. 4.4.4 Off-mass-shell $K^-\pi^-$ moments with m = 0 as a function of the $K^-\pi^-$ effective mass.

The moments have been determined from events of the reaction $K^- + p \to K^- + \pi^- + p + \pi^+$ that obey the conditions $1.14 < m_{p\pi^+} < 1.36$ GeV/c^2 and $-t_{K^- \to K^-\pi^-} < 0.4$ (GeV/c)^2. They have been avaraged over these regions. The errors are statistical. The triangles indicate the values of $\langle Y_1^0 \rangle$ and $\langle Y_2^0 \rangle$ calculated with the phase shifts determined in section 4.4.4.

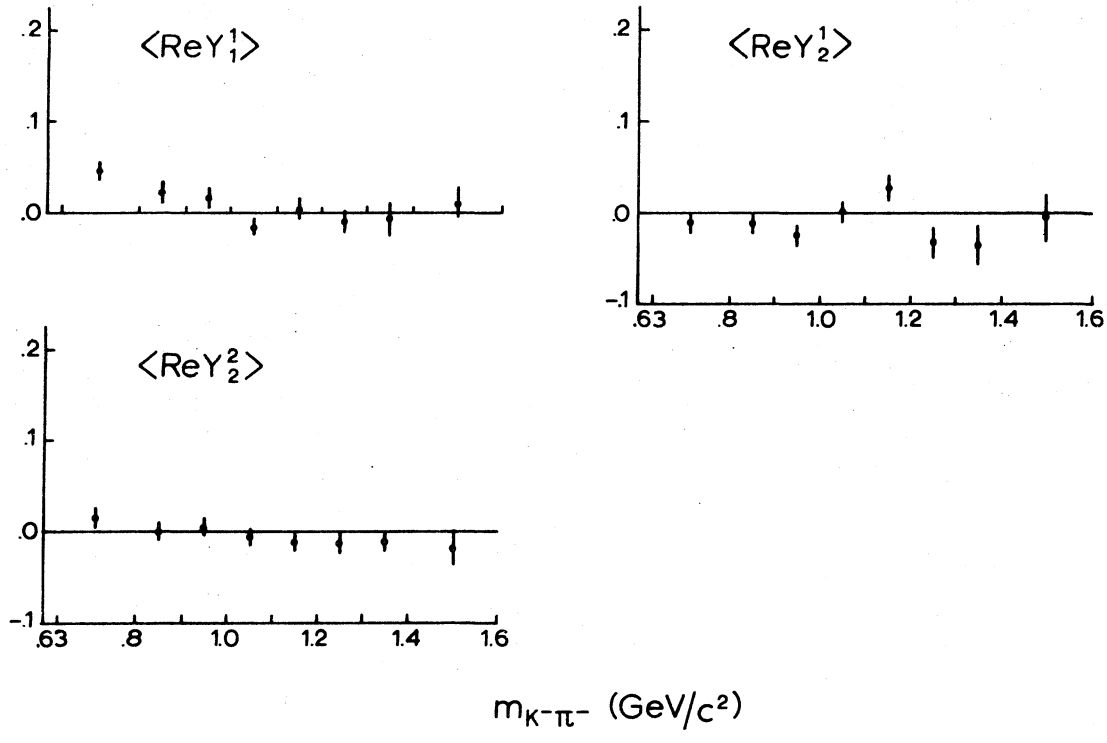

Fig. 4.4.5 Off-mass-shell $K^-\pi^-$ moments with $m \neq 0$ as a function of the $K^-\pi^-$ effective mass.

$\langle Y^0_4 \rangle$ up to $\langle Y^0_8 \rangle$ for $m_{K^-\pi^-}$ around 1.1 GeV/c^2, it must be realized that the errors on the $\langle Y^0_L \rangle$ in equivalent mass regions are not independent of each other. The moments up to $\langle Y^0_6 \rangle$ for $m_{K^-\pi^-}$ around 1.5 GeV/c^2 are consistently higher than zero. The moments with $m \neq 0$ are compatible with zero over the $K^-\pi^-$ effective mass region considered.

4.4.4 PHASE SHIFTS DETERMINED WITH OFF-MASS-SHELL MOMENTS

The s- and p-wave phase shifts δ^3_0 and δ^3_1 are determined with a χ^2 method for different $K^-\pi^-$ effective mass regions up to 1.2 GeV/c^2 using the relations 4.4.5, 4.4.6 and 4.4.7. The $\sigma_{K^-\pi^-}$ values used are those which have been determined in section 4.3 (table 4.3.2; N = 2). For the moments $\langle Y^0_1 \rangle$ and $\langle Y^0_2 \rangle$, the off-mass-shell values determined in section 4.4.3 have been used first. In section 4.5.5 the phase shifts are determined with the use of moments which have been extrapolated to the pion pole.

The results of these one-constraint fits are shown in table 4.4.2 and figure 4.4.6. The errors are statistical. To obtain a more realistic estimate of the physical errors, the statistical errors multiplied by $\sqrt{\chi^2/ND}$ are also shown in figure 4.4.6 by the dashed lines.

Both phase shifts δ_0^3 and δ_1^3 have the same sign. This sign can not be determined in this analysis because the formulas 4.4.5 through 4.4.7 are invariant under a simultaneous change of sign for δ_0^3 and δ_1^3. In the present work the negative sign has been chosen. Evidence for this choice has been found by Yuta et al.[4.24] and by Bingham et al.[4.25].

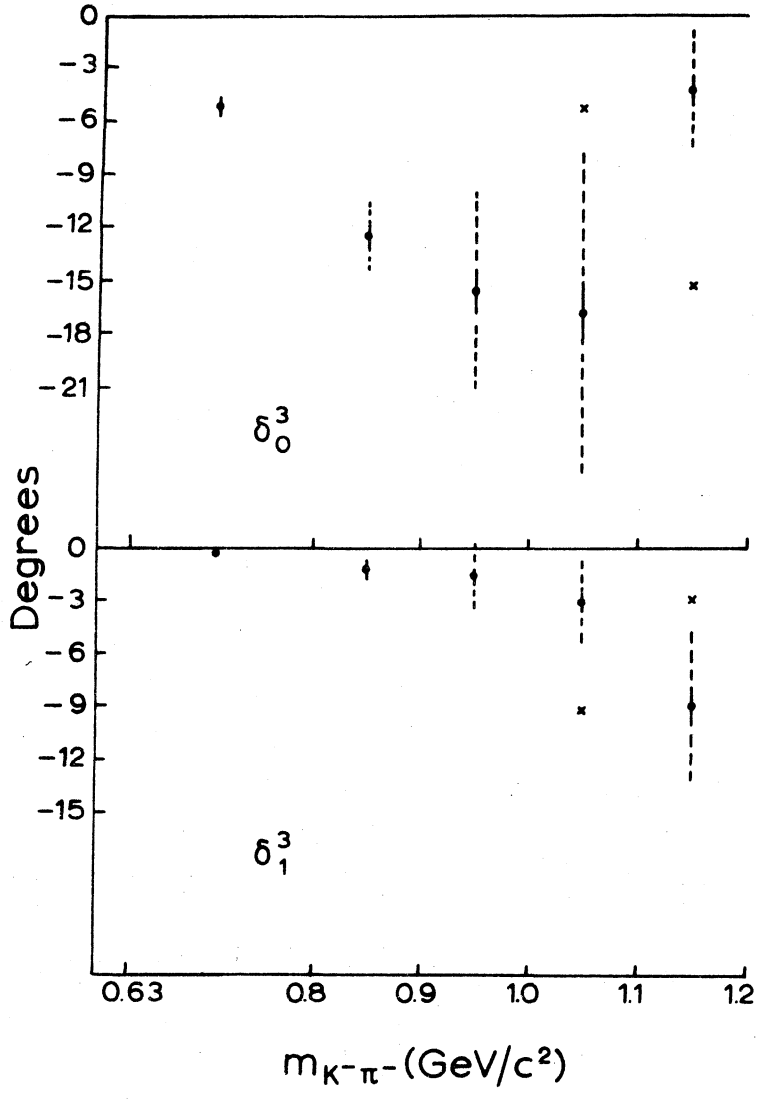

Fig. 4.4.6 The phase shifts δ_0^3 and δ_1^3 as a function of the $K^-\pi^-$ effective mass, for I = 3/2 $K^-\pi^-$ scattering as determined in the reaction $K^- + p \rightarrow K^- + \pi^- + \Delta^{++}(1236)$.
The phase shifts have been obtained from the on-mass-shell elastic $K^-\pi^-$ scattering cross section of table 4.3.2 (N = 2) and the off-mass-shell moments of table 4.4.1.
x indicates the ambiguous solution that has been found for $m_{K^-\pi^-} > 1.0$ GeV/c^2.
The dashed lines are obtained by multiplying the statistical errors by $\sqrt{\chi^2/ND}$.

Table 4.4.2 Phase shifts δ_0^3 and δ_1^3 as a function of the $K^-\pi^-$ effective mass, for the I = 3/2 $K^-\pi^-$ elastic scattering as determined in the reaction $K^- + p \rightarrow K^- + \pi^- + \Delta^{++}(1236)$.
The phase shifts have been obtained from the on-mass-shell elastic $K^-\pi^-$ scattering cross section of table 4.3.2 (N = 2) and the off-mass-shell moments of table 4.4.1.

$m_{K^-\pi^-}$ (GeV/c^2)	number of events	$-\delta_0^3$ (degrees)	$-\delta_1^3$ (degrees)	χ^2 (ND=1)	ambiguous solution δ_0^3 (degrees)	δ_1^3 (degrees)	χ^2 (ND=1)
< 0.8	314	5.1 ±0.5	0.3 ±0.1	0.4			
0.8 - 0.9	296	12.4 ±0.9	1.2 ±0.3	4.0			
0.9 - 1.0	291	15.6 ±1.2	1.5 ±0.4	21.4			
1.0 - 1.1	330	16.7 ±1.7	2.9 ±0.5	26.2	5.3	9.4	57
1.1 - 1.2	218	4.3 ±0.9	8.8 ±1.2	13.1	15.3	3.1	39

For $m_{K^-\pi^-} < 1.1$ GeV/c^2, $|\delta_0^3|$ increases from 5^o to 17^o with increasing $m_{K^-\pi^-}$. In that mass region $|\delta_1^3|$ remains below 3^o. For $1.1 < m_{K^-\pi^-} < 1.2$ GeV/c^2, $|\delta_0^3|$ decreases to 4^o, while $|\delta_1^3|$ increases to 9^o.
In the two highest mass regions, there are two ambiguous solutions. The appearance of ambiguous solutions for the phase shifts is related to the values of the experimental moments $\langle Y_1^0 \rangle$ and $\langle Y_2^0 \rangle$. This is shown in figure 4.4.7.
The calculated values of $\langle Y_1^0 \rangle$ and $\langle Y_2^0 \rangle$, using the best fitted values for δ_0^3 and δ_1^3, are shown in table 4.4.3; In figure 4.4.4 they are indicated with triangles. The calculated values of $\sigma_{K^-\pi^-}$ agree with the experimental values of section 4.3 and are completely within the errors, as can be seen from table 4.4.3.
From the high values of χ^2 it can be seen that the fit is not very satisfactory, whereas figure 4.4.4 shows that this is mainly due to the $\langle Y_2^0 \rangle$ moment. It will be investigated in section 4.5 whether and to what extend the results of the fit are sensitive to:

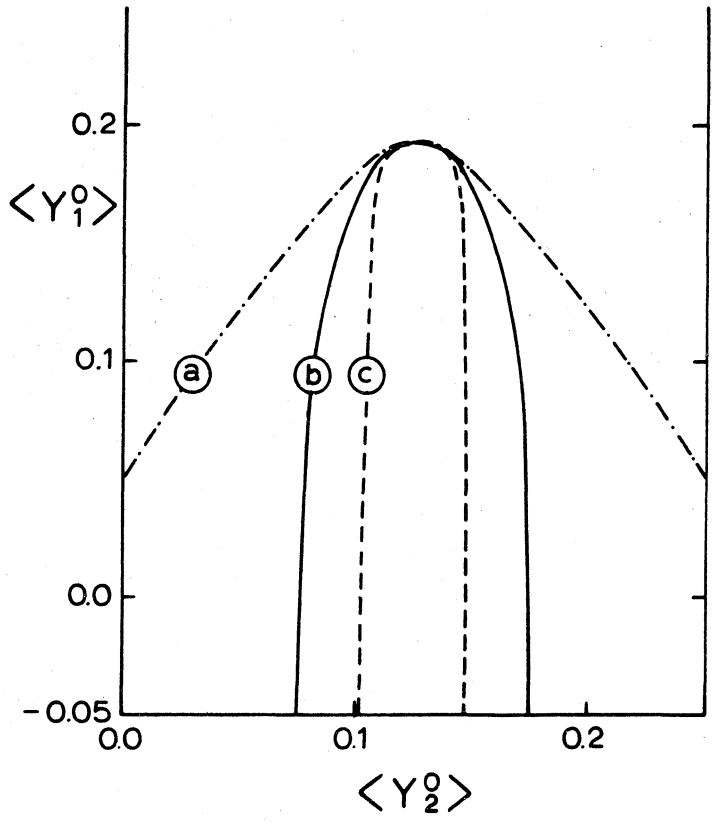

Figure 4.4.7 Relation between the appearance of ambiguous solutions for the phase shifts and the moments $\langle Y_1^0 \rangle$ and $\langle Y_2^0 \rangle$.
The phase shifts have been calculated from the formulas 4.4.5 through 4.4.7 using the experimental value $\sigma_{K^-\pi^-}$ = (2.8±0.5)mb found for $1.0 < m_{K^-\pi^-} < 1.1$ GeV/c^2. This value has been fixed while the values of $\langle Y_1^0 \rangle$ and $\langle Y_2^0 \rangle$ are varied, using fixed experimental errors.
Inside the region limited by curve "a", there are always ambiguous solutions for the phase shifts. Inside the regions limited by the curves "b" and "c", the ratio of the χ^2 of the ambiguous solutions is smaller than 5 and 2 respectively.

a. the choice from the solutions of the ambiguous events (sect. 4.5.1);
b. background processes (sect. 4.5.2);
c. inelastic processes of the type $K^- + \pi^- \rightarrow K^- + \pi^-$ + neutrals (sect. 4.5.3);
d. Coulomb scattering (sect. 4.5.4);
e. the use of the off-mass-shell moments instead of the on-mass-shell moments (sect. 4.5.5).

First the results are compared with those obtained in a K^-n experiment.

Table 4.4.3 The values of $\sigma_{K^-\pi^-}$ (on-mass-shell), $\langle Y_1^0 \rangle$ and $\langle Y_2^0 \rangle$ (off-mass-shell) that have been used for the determination of the phase shifts, and the corresponding values calculated from the best fitted phase shifts

$m_{K^-\pi^-}$	$\sigma_{K^-\pi^-}$ (mb)		$\langle Y_1^0 \rangle$		$\langle Y_2^0 \rangle$	
(GeV/c^2)	input for fit	calculated from δ_0^3, δ_1^3	input for fit	calculated from δ_0^3, δ_1^3	input for fit	calculated from δ_0^3, δ_1^3
< 0.8	1.82 ±0.37	1.82	0.054 ±0.016	0.055	0.013 ±0.016	0.002
0.8-0.9	3.49 ±0.50	3.49	0.083 ±0.017	0.088	0.040 ±0.017	0.007
0.9-1.0	3.36 ±0.50	3.37	0.075 ±0.018	0.088	0.089 ±0.018	0.007
1.0-1.1	2.80 ±0.55	2.84	0.130 ±0.016	0.152	0.105 ±0.017	0.021
1.1-1.2	1.78 ±0.47	1.78	0.126 ±0.022	0.147	0.157 ±0.022	0.234

4.4.5 COMPARISON WITH THE RESULTS FROM A K^-n EXPERIMENT

A similar analysis has been carried out in the reaction

$$K^- + n \rightarrow K^- + \pi^- + p \qquad (4.4.9)$$

with K^- mesons of 3 GeV/c incident momentum[4,23]. The assumption of one-pion-exchange in this reaction leads to the diagram of figure 4.4.8.

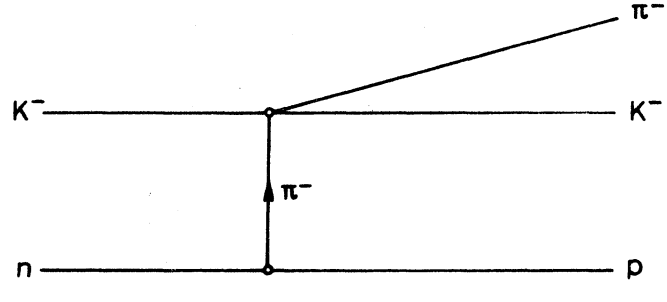

Fig. 4.4.8 The one-pion-exchange diagram for the reaction $K^- + n \rightarrow K^- + \pi^- + p$

From this study the results of that part of the analysis without corrections for background processes are shown in table 4.4.4 and figure 4.4.9. Comparison with the data of figure 4.4.6 shows that there is a reasonable agreement between both analyses.

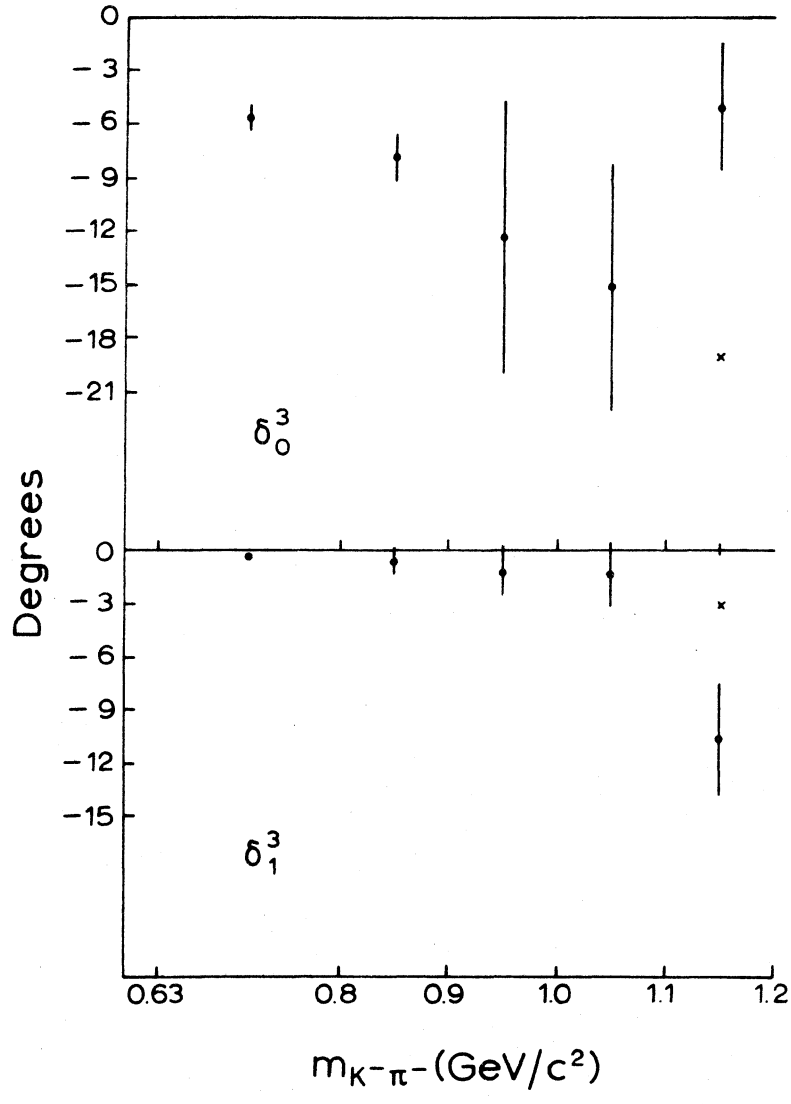

Fig. 4.4.9 The phase shifts δ_0^3 and δ_1^3 as a function of the $K^-\pi^-$ effective mass, for the I = 3/2 $K^-\pi^-$ elastic scattering as determined in the reaction $K^- + n \rightarrow K^- + \pi^- + p$ [4.23].
The phase shifts have been obtained from the on-mass-shell elastic $K^-\pi^-$ scattering cross section and the off-mass-shell moments, without corrections for background processes.
x indicates the ambiguous solution for $1.1 < m_{K^-\pi^-} < 1.2$ GeV/c^2.

Table 4.4.4 Phase shifts δ_0^3 and δ_1^3 as a function of the $K^-\pi^-$ effective mass, for the I = 3/2 $K^-\pi^-$ elastic scattering, as determined in the reaction $K^- + n \to K^- + \pi^- + p$[4.23].
The phase shifts have been obtained from the on-mass-shell elastic $K^-\pi^-$ scattering cross section and the off-mass-shell moments, without corrections for background processes.

$m_{K^-\pi^-}$ (GeV/c^2)	number of events	$-\delta_0^3$ (degrees)	$-\delta_1^3$ (degrees)	χ^2 (ND=1)	ambiguous solution δ_0^3 (degrees)	ambiguous solution δ_1^3 (degrees)
< 0.8	57	5.6 ±0.7	0.3 ±0.2	0.1		
0.8 - 0.9	88	7.9 ±1.4	0.6 ±0.8	8.3		
0.9 - 1.0	111	12.4 ±7.9	1.1 ±1.4	23.0		
1.0 - 1.1	166	15.2 ±6.8	1.4 ±1.8	23.0		
1.1 - 1.2	188	5.1 ±3.7	10.7 ±3.2	10.5	19 ±3	3 ±3

In both analyses the upper vertex in the diagram of the π-exchange (fig. 4.3.2 and 4.4.8 respectively) is the same, whereas the lower vertex is different. The agreement between both analyses is an indication that $K^-\pi^-$ interaction may be studied as described above; the assumption of the factorization of the residue of the reaction amplitude at the pole (sect. 4.3.1) is correct. The behaviour of the particles in the upper vertex is independent of the process in the lower vertex.

4.5 REFINEMENTS OF THE ANALYSIS

4.5.1 AMBIGUOUS EVENTS

The percentage of events ambiguous for the interchange of the K^- and π^- mesons is 9.0% in the sample of events of reaction 4.1.2. Using the conditions on the $p\pi^+$ effective mass 4.2.4, and the four-momentum transfer 4.2.5, the percentage of the ambiguous events grows to 16.6%. The influence of the choice of solution, used for these events, on the results has been investigated.

Figure 4.5.1 shows the distributions of the cos θ_K for ambiguous events when the fit with the smallest or the largest χ^2 is chosen. The influence of the χ^2 choice on the results for the moments obtained from the whole sample of events is small: the change in the results remains easily within the statistical errors. The influence on the fit of the phase shifts is negligible.

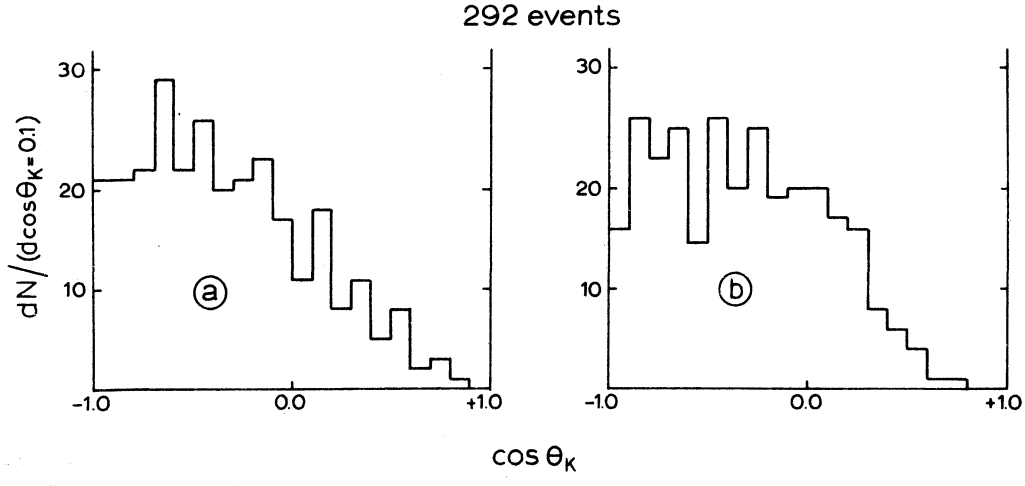

Fig. 4.5.1 The distribution of the cos θ_K, defined in figure 4.4.1, of the internally ambiguous events in the reaction $K^- + p \to K^- + \pi^- + p + \pi^+$, obeying the conditions $1.14 < m_{p\pi^+} < 1.36$ GeV/c^2 and $-t_{K^- \to K^-\pi^-} < 0.4$ (GeV/c)^2 with the choice of
a. the smallest χ^2
b. the largest χ^2.

4.5.2 BACKGROUND PROCESSES

The fractions of different processes, obtained with the mass fit on the reaction 4.1.2, as previously mentioned in section 4.2.3, are summarized in table 4.5.1. - Since the investigation of the background processes has been done in an earlier stage of the analysis, the samples used are smaller. - With this fit, 94.2% of the events have been classified as being produced via a resonance. The $K^{*0}(890)$ is present in 42.1% of all the cases.

Table 4.5.1 The fractions of the different processes involved in the reaction $K^- + p \rightarrow K^- + \pi^- + p + \pi^+$, obtained from a mass fit with the program MAVE2CD[4.15].

Process	Fraction * 100
$K^- + p \rightarrow Y^{*0}(1525) + \rho(755)$	3.7 ± 0.5
$Y^{*0}(1525) + \pi^+ + \pi^-$	0.3 ± 0.3
$Y^{*0}(1810) + \rho(755)$	6.3 ± 0.8
$Y^{*0}(2300) + \pi^+ + \pi^-$	8.4 ± 1.7
$K^{*0}(890) + p + \pi^-$	0.9 ± 2.0
$K^{*0}(890) + N^{*0}(1236)$	10.6 ± 1.1
$K^{*0}(890) + N^{*0}(1680)$	7.0 ± 1.1
$K^{*-}(1422) + p$	9.4 ± 1.2
$\hookrightarrow K^{*0}(890) + \pi^-$	
$Q^-(1330) + p$	14.2 ± 1.3
$\hookrightarrow K^{*0}(890) + \pi^-$	
$Q^-(1330) + p$	2.4 ± 0.8
$\hookrightarrow \rho(755) + K^-$	
$\Delta^{++}(1236) + K^- + \pi^-$	31.0 ± 1.5
Total	94.2

The condition on the $p\pi^+$ effective mass 4.2.4 does not yield a pure sample of events in which the $\Delta^{++}(1236)$ resonance is produced according to reaction 4.1.1. The condition on the four-momentum transfer 4.2.5 strongly reduces the contribution of events in which Y^* resonances are produced. However, the sample of events which has been analysed contains a substantial number of events in which a $K^{*0}(890)$ resonance is produced (fig. 4.5.2).
Therefore, the influence of the $K^{*0}(890)$ background on the results has been studied. This was done by giving each event the weight 1 - $BW(K^{*0}(890))$, where

$$BW(K^{*0}(890)) = C \frac{\Gamma}{(m^2_{K^-\pi^+} - m_0^2)^2 + \Gamma^2 m_0^2} \qquad (4.5.1)$$

where m_0 = 892.6 MeV/c^2, the resonance mass and

$$\Gamma = \Gamma_0 \frac{m_0}{m_{K^-\pi^+}} \cdot \frac{p^3(m_{K^-}, m_{\pi^+}, m_{K^-\pi^+})}{p^3(m_{K^-}, m_{\pi^+}, m_0)}$$

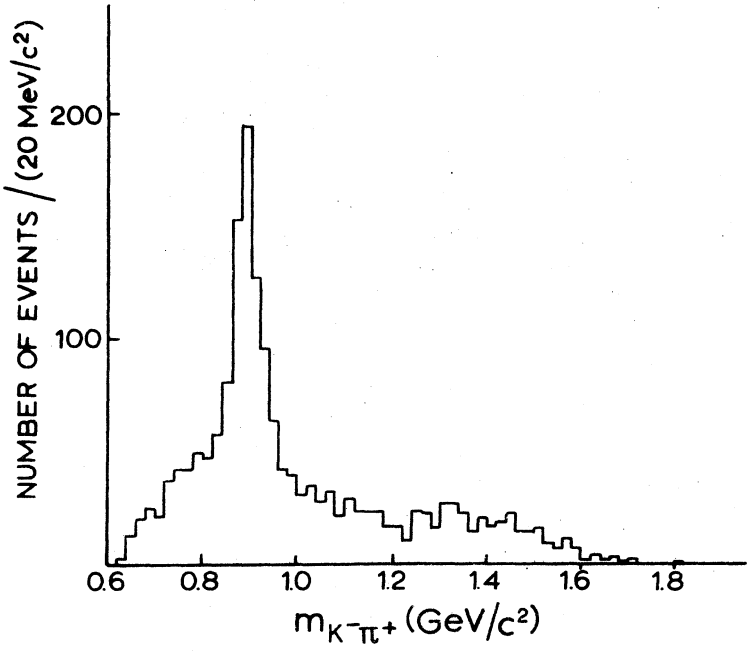

Figure 4.5.2 The distribution of the $K^-\pi^+$ effective mass in the reaction $K^- + p \to K^- + \pi^- + p + \pi^+$ for events which obey the conditions $1.14 < m_{p\pi^+} < 1.36$ GeV/c^2 and $-t_{K^- \to K^-\pi^-} < 0.4$ $(GeV/c)^2$

Figure 4.5.3 The distribution of the $K^-\pi^+$ effective mass $m_{K^-\pi^+}$ in the reaction $K^- + p \to K^- + \pi^- + p + \pi^+$. The shaded area indicates the distribution of $m_{K^-\pi^+}$ when the events are weighed by 1 - BW(K^{*o}(890)), where BW(K^{*o}(890)) is given by formula 4.5.1.

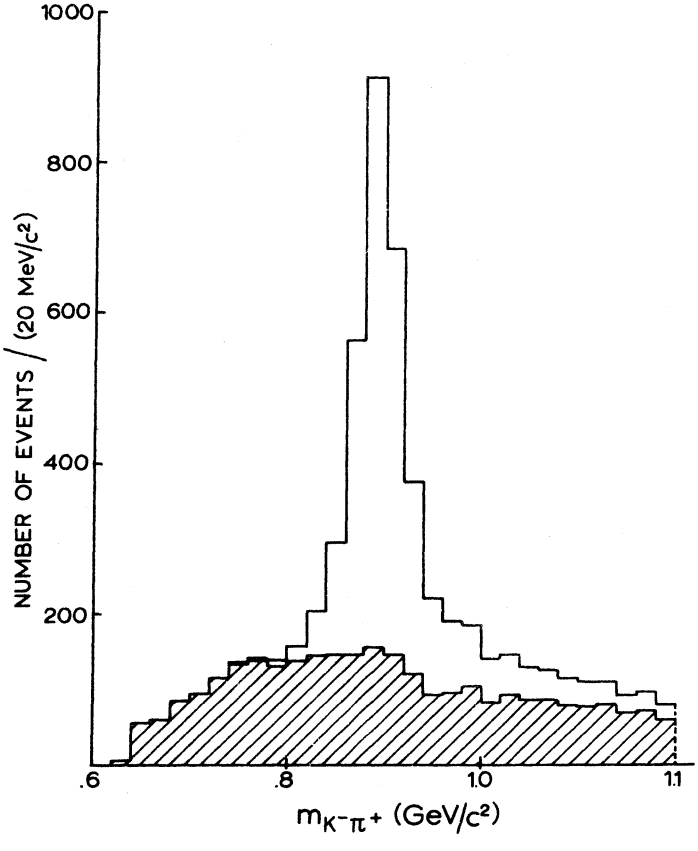

where Γ_0 = 50.3 MeV/c^2, the width of the resonance, and the momentum

$$p(x,y,z) = \frac{1}{2z}\left[(z-x-y)(z-x+y)(z+x-y)(z+x+y)\right]^{\frac{1}{2}}$$

The normalization constant C is chosen, such that the $K^{*o}(890)$ peak disappears in the $m_{K^-\pi^+}$ distribution of the total sample of events of reaction 4.1.2, as can be seen in figure 4.5.3.

It should be remarked that this procedure is not intended to purify the sample used for the analysis. Only the events close to the mass of the $K^{*o}(890)$ resonance have a lower weight than the events further away from the resonance region. Hence, if the background caused by $K^{*o}(890)$-events, has a considerable influence on the results of the extrapolation analyses, this influence should be reduced in the way described above.

The distributions of the cos θ_K and ϕ_K for events weighed by 1-BW($K^{*o}(890)$) are shown in figure 4.5.4. The distribution of the cos θ_K does not differ much from the cos θ_K distribution of the complete sample (fig. 4.4.2). The distribution of ϕ_K has become somewhat flatter.

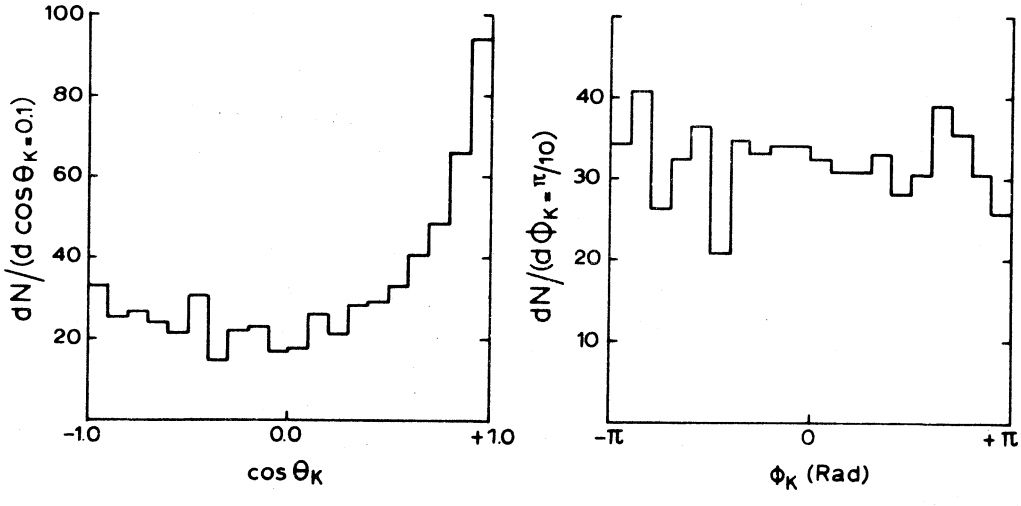

Fig. 4.5.4 The distributions of the cos θ_K and ϕ_K for events weighed by 1-BW($K^{*o}(890)$), where BW($K^{*o}(890)$) is given by formula 4.5.1. The events obey the conditions 1.14 < $m_{p\pi^+}$ < 1.36 GeV/c^2 and $-t_{K^- \to K^-\pi^-} < 0.4$ (GeV/c)^2.

Figure 4.5.5 shows the influence of this procedure on the results for $\langle Y_1^0 \rangle$ and $\langle Y_2^0 \rangle$. Again the values for $\langle Y_1^0 \rangle$ and $\langle Y_2^0 \rangle$ which are calculated from the fitted phase shifts δ_0^3 and δ_1^3 are indicated by triangles. It can be seen from

this figure that the background of $K^{*o}(890)$-events has no pronounced influence on the results and the poor fit of the phase shifts.

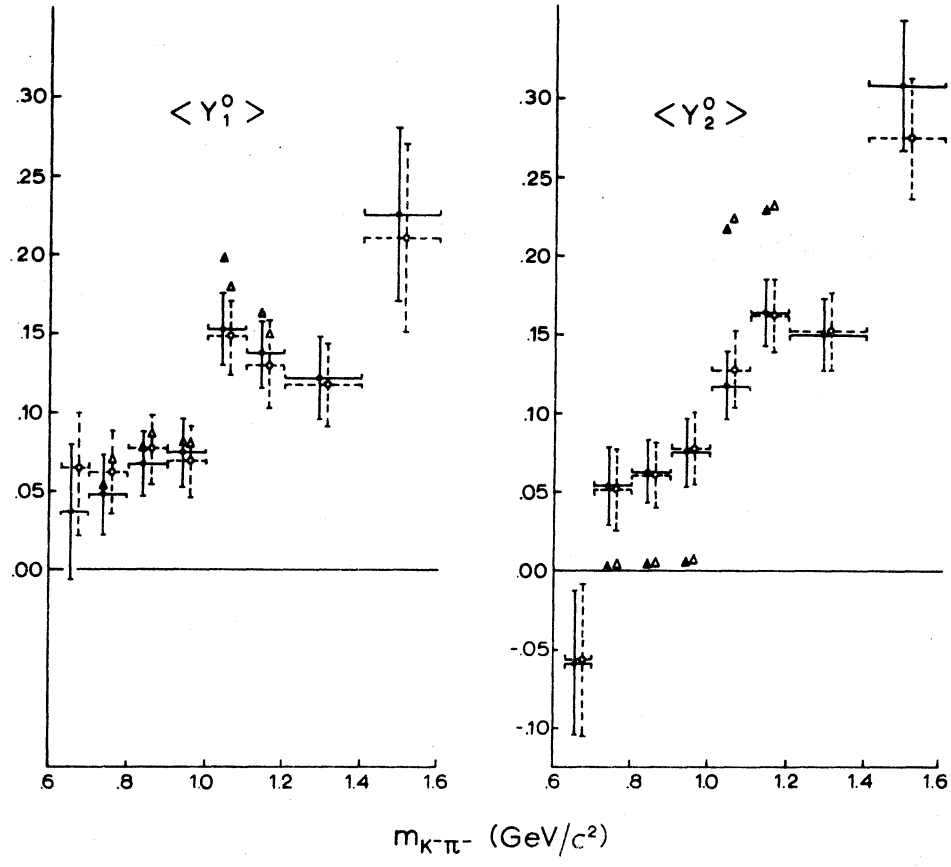

Fig. 4.5.5 The off-mass-shell moments $\langle Y_1^0 \rangle$ and $\langle Y_2^0 \rangle$ as a function of the $K^-\pi^-$ effective mass;

—●— all events with weight 1;

-o- all events with weight 1-BW($K^{*o}(890)$), where BW($K^{*o}(890)$ is given by formula 4.5.1;

▲ values of $\langle Y_1^0 \rangle$ and $\langle Y_2^0 \rangle$ calculated with the best fitted values of δ_0^3 and δ_1^3 in the formulas 4.4.5 - 4.4.7, giving all events weight 1;

▲ idem, but giving all events weight 1-BW($K^{*o}(890)$).

Another effect which should be mentioned is the kinematic correlation between the $p\pi^+\pi^-$ effective mass and the cos θ_K. This correlation is shown in figure 4.5.6, and may be described with the formula

$$m^2_{p\pi^+\pi^-} = A(m^2_{K^-\pi^-}) - B(m^2_{K^-\pi^-},\ t_{p\Delta})\ \cos\theta_K +$$

$$- C(m^2_{K^-\pi^-},\ t_{p\Delta})\ \sin\theta_K \cos\phi_K \qquad (4.5.2)$$

where $m_{p\pi^+\pi^-}$ is the $p\pi^+\pi^-$ effective mass, $t_{p\Delta}$ is the four-momentum transfer squared $t_{p \to \Delta^{++}(1236)}$. A, B and C are simple functions of $m^2_{K^-\pi^-}$ and $t_{p\Delta}$. (These functions and the proof of relation 4.5.2 are described in detail in reference 4.23). Figure 4.5.7 shows the distribution of the $p\pi^+\pi^-$ effective mass.

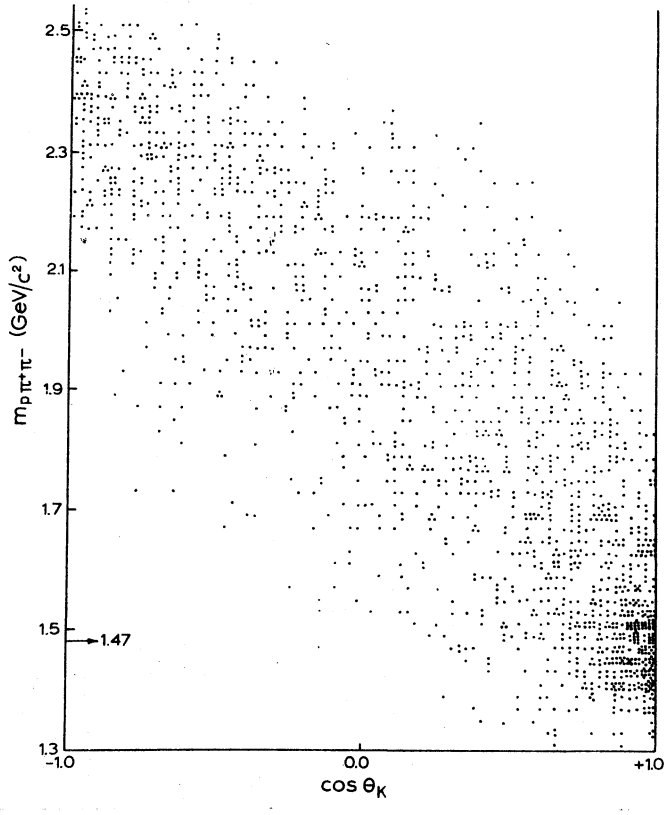

Figure 4.5.6 The correlation between the cos θ_K distribution and the $p\pi^+\pi^-$ effective mass in the reaction $K^- + p \to K^- + \pi^- + p + \pi^+$. The events obey the conditions $1.14 < m_{p\pi^+} < 1.36$ GeV/c^2 and $-t_{K^- \to K^-\pi^-} < 0.4$ (GeV/c)^2.

The accumulation in the region of the forward produced events (cos $\theta \approx +1$) is correlated with low $p\pi^+\pi^-$ effective masses, around 1470 GeV/c^2, which is the mass of the $N^{*+}(1470)$ resonance. This might lead to unresolvable ambi-

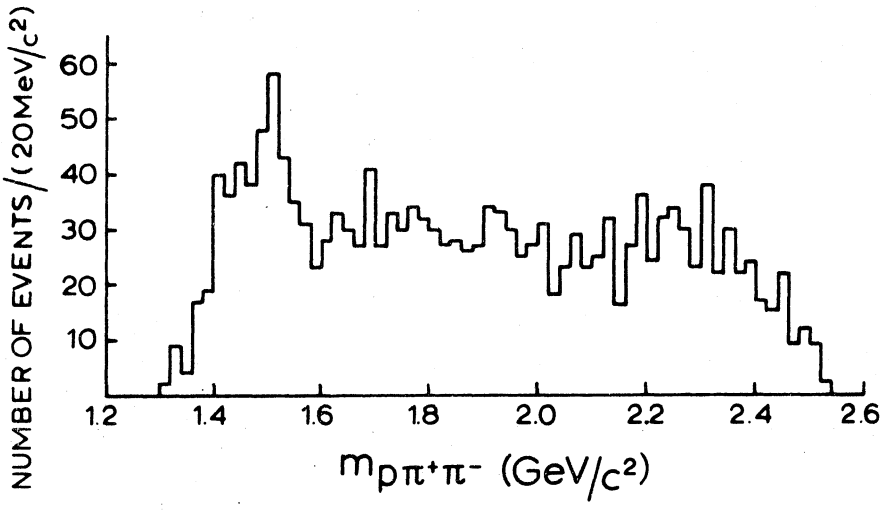

Figure 4.5.7 The distribution of the $p\pi^+\pi^-$ effective mass in the reaction $K^- + p \rightarrow K^- + \pi^- + p + \pi^+$.
The events obey the conditions $1.14 < m_{p\pi^+} < 1.36$ GeV/c^2 and $-t_{K^- \rightarrow K^-\pi^-} < 0.4$ (GeV/c)^2.

guities between the mechanisms in which a $\Delta^{++}(1236)$ resonance is produced and those in which a $N^{*+}(1470)$ resonance is produced. Although the contamination of events in which a $N^{*+}(1470)$ resonance is produced is very small in the reaction 4.1.2, a rough investigation of a possible background effect due to this resonance has been made. It has been found that the moments may be influenced by this background process, but the effect on the fit of the phase shifts is within the errors.

A more precise investigation on this subject has been made by Bakker[4.23] in the reaction 4.4.9. In that case, the $p\pi^-$ effective mass corresponds with the $p\pi^+\pi^-$ effective mass of this study. The formula 4.5.2 has the same structure in both cases. Bakker generated a 10% background contribution with a Monte Carlo procedure, using the experimental knowledge on the $\Delta^0(1236)$ resonance. Subtracting this background, he found no significant changes in the results for the phase shifts. The calculated distribution of the ϕ_K showed bumps at $\phi_K \approx \pm 0.5$ rad due to this background. That result agreed with the experimental ϕ_K distribution of that analysis, which showed a slight anisotropy.

The presence of analoguous bumps in the ϕ_K distribution of the present experiment (fig. 4.4.2) is less evident, and the distribution of the ϕ_K with weighed events (fig. 4.5.3) may be interpreted to be isotropic, as expected from a pure OPE. This may indicate that the amount of background in the

sample which has been analysed, due to events in which a $N^{*++}(1470)$ resonance is produced, is smaller than the corresponding background contribution in the analysis of Bakker, and that the influence on the results of the phase shifts is not significant indeed.

It may be concluded that the background processes mentioned are not responsible for the unsatisfactory fit of the phase shifts.

4.5.3 INELASTIC PROCESSES OF THE TYPE $K^- + \pi^- \rightarrow K^- + \pi^- +$ NEUTRALS

The missing mass spectrum of the $\Delta^{++}(1236)$ resonance in the peripheral reaction

$$K^- + p \rightarrow \Delta^{++}(1236) + X^{--} \qquad (4.5.3)$$

has been studied. The events with $\Delta^{++}(1236)$ production have been selected with the condition $1.14 < m_{p\pi^+} < 1.36$ GeV/c^2, and the peripheral processes have been selected with the condition $-t_{p \rightarrow \Delta^{++}(1236)} < 0.4$ (GeV/c)^2.

It has been found that for $m_{X^{--}} < 1.2$ GeV/c^2 only the peripheral production of $K^0\pi^-\pi^0\Delta^{++}(1236)$ is not negligible. At higher effective masses for X^{--}, the production of more pions becomes important. Figure 4.5.8 shows the $K^-\pi^-$ and $K^-\pi^-\pi^0$ effective mass distributions for events that obey the conditions on the $p\pi^+$ effective mass and the four-momentum transfer. In the mass region $0.9 < m_X < 1.0$ GeV/c^2, the peripheral $K^-\pi^-\pi^0\Delta^{++}(1236)$ production amounts 8% of the peripheral $K^-\pi^-\Delta^{++}(1236)$ production. This amount grows to 30% in the mass region $1.1 < m_X < 1.2$ GeV/c^2.

Hence the inelastic processes $K^-\pi^- \rightarrow K^0\pi^-\pi^0$ may influence the results of the fit on the phase shift substantially at $K^-\pi^-$ effective masses higher than 0.9 GeV/c^2. - If these processes are present, the formulas 4.4.1 etc. must contain absorption parameters. - Within this context, it is useful to determine the inelastic $K^-\pi^- \rightarrow K^0\pi^-\pi^0$ cross sections. For this purpose a larger sample of events is required.

4.5.4 COULOMB SCATTERING

The calculated cos θ_K distribution due to the $K^-\pi^-$ Coulomb scattering shows an asymmetry in the forward direction. However, the contribution to the experimental cos θ_K distributions of figure 4.4.3 is less than 1.6% in the lowest $K^-\pi^-$ effective mass region and 0.1% in the highest mass region. The influence of the $K^-\pi^-$ Coulomb scattering on the results of the fit on the phase shifts is negligible.

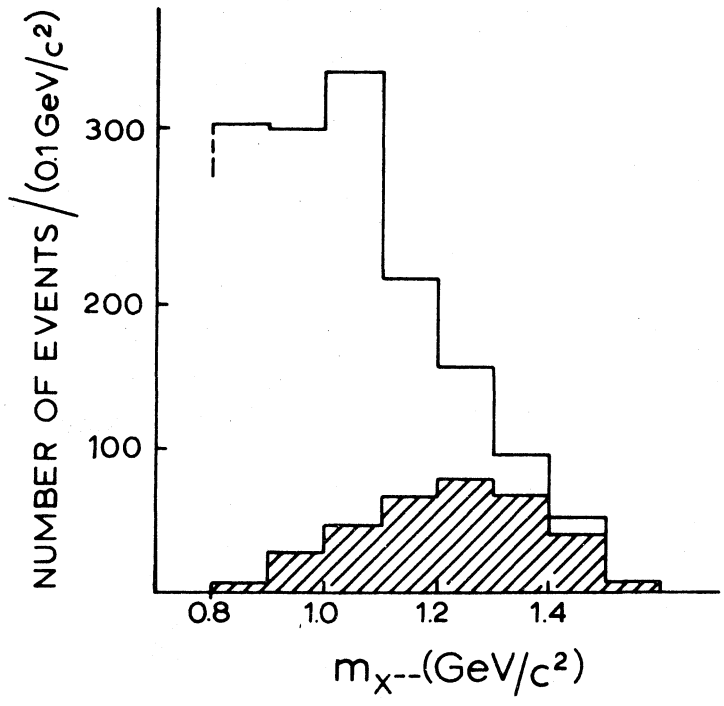

Fig. 4.5.8 The spectra of the $K^-\pi^-$ and $K^-\pi^-\pi^o$ effective masses in the reactions $K^- + p \to K^- + \pi^- + p + \pi^+ + (\pi^o)$.
(X^{--} stands for $K^-\pi^-$ (unshaded) and $K^-\pi^-\pi^o$ (shaded) respectively.)
The events obey the conditions $1.14 < m_{p\pi^+} < 1.36$ GeV/c^2 and $-t_{p \to p\pi^+} < 0.4$ (GeV/c)^2.

4.5.5 EXTRAPOLATION OF THE MOMENTS

The off-mass-shell moments $\langle Y_1^0 \rangle$ and $\langle Y_2^0 \rangle$, discussed in section 4.4.3, are extrapolated to the pion pole $t_{K^- \to K^-\pi^-} = \mu^2$. This has been done both linearly and quadratically in $(t_{K^- \to K^-\pi^-} - \mu^2)$. In figure 4.5.9 the moments $\langle Y_1^0 \rangle$ and $\langle Y_2^0 \rangle$ are shown as a function of $t_{K^- \to K^-\pi^-}$, and also the extrapolation curves obtained with a χ^2 method. For reasons of statistics, the $K^-\pi^-$ effective mass regions have been chosen somewhat larger than those in the previous sections.

Both the linearly and the quadratically extrapolated moments $\langle Y_1^0 \rangle$ and $\langle Y_2^0 \rangle$, as a function of the $K^-\pi^-$ effective mass, are shown in figure 4.5.10. For comparison, the off-mass-shell moments in the concerning mass regions are also shown. The figure shows that the quadratically extrapolated $\langle Y_1^0 \rangle$ moment is compatible with zero. This is also the case for the $\langle Y_2^0 \rangle$ moment up to $m_{K^-\pi^-} = 1.1$ GeV/c^2.

4.5.6 PHASE SHIFTS DETERMINED WITH THE EXTRAPOLATED MOMENTS

The phase shifts δ_0^3 and δ_1^3, obtained from $\sigma_{K^-\pi^-}$ and the moments $\langle Y_1^0 \rangle$ and $\langle Y_2^0 \rangle$

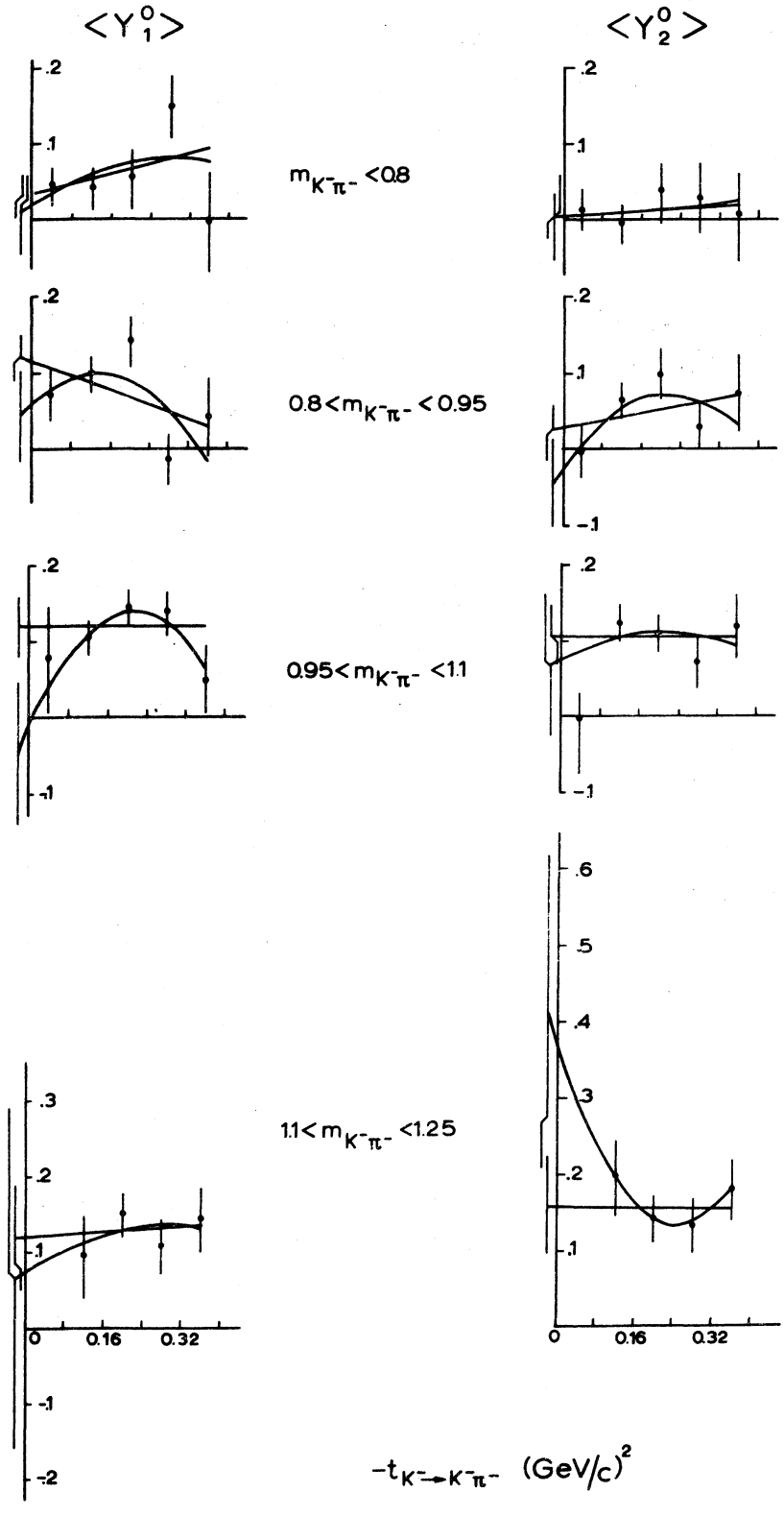

Figure 4.5.9 The $K^-\pi^-$ moments $\langle Y_1^0 \rangle$ and $\langle Y_2^0 \rangle$ as a function of the four-momentum transfer squared $t_{K^- \to K^-\pi^-}$, for different regions of the $K^-\pi^-$ effective mass.

The curves show the linear and quadratic extrapolations of the moments to the pion pole $t_{K^- \to K^-\pi^-} = m_\pi^2$.

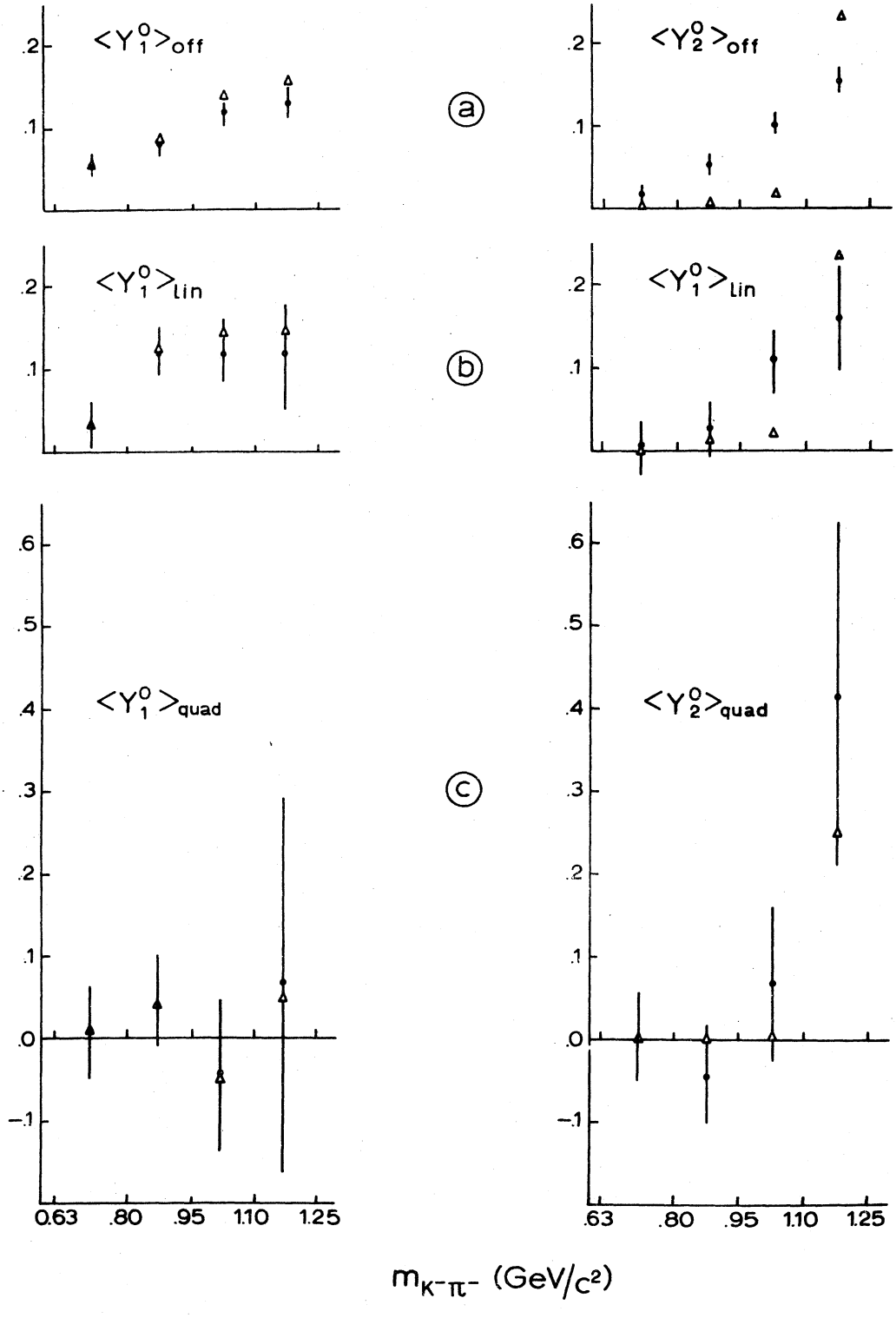

Figure 4.5.10 The $K^-\pi^-$ moments $\langle Y_1^0 \rangle$ and $\langle Y_2^0 \rangle$ as a function of the $K^-\pi^-$ effective mass

a. off-mass-shell;

b. linearly extrapolated;

c. quadratically extrapolated;

The triangles indicate the values of $\langle Y_1^0 \rangle$ and $\langle Y_2^0 \rangle$ calculated with the best fitted values of δ_0^3 and δ_1^3 in the formulas 4.4.5-4.4.7.

- off-mass-shell, linearly extrapolated and quadratically extrapolated - are shown in table 4.5.2 and figure 4.5.11.

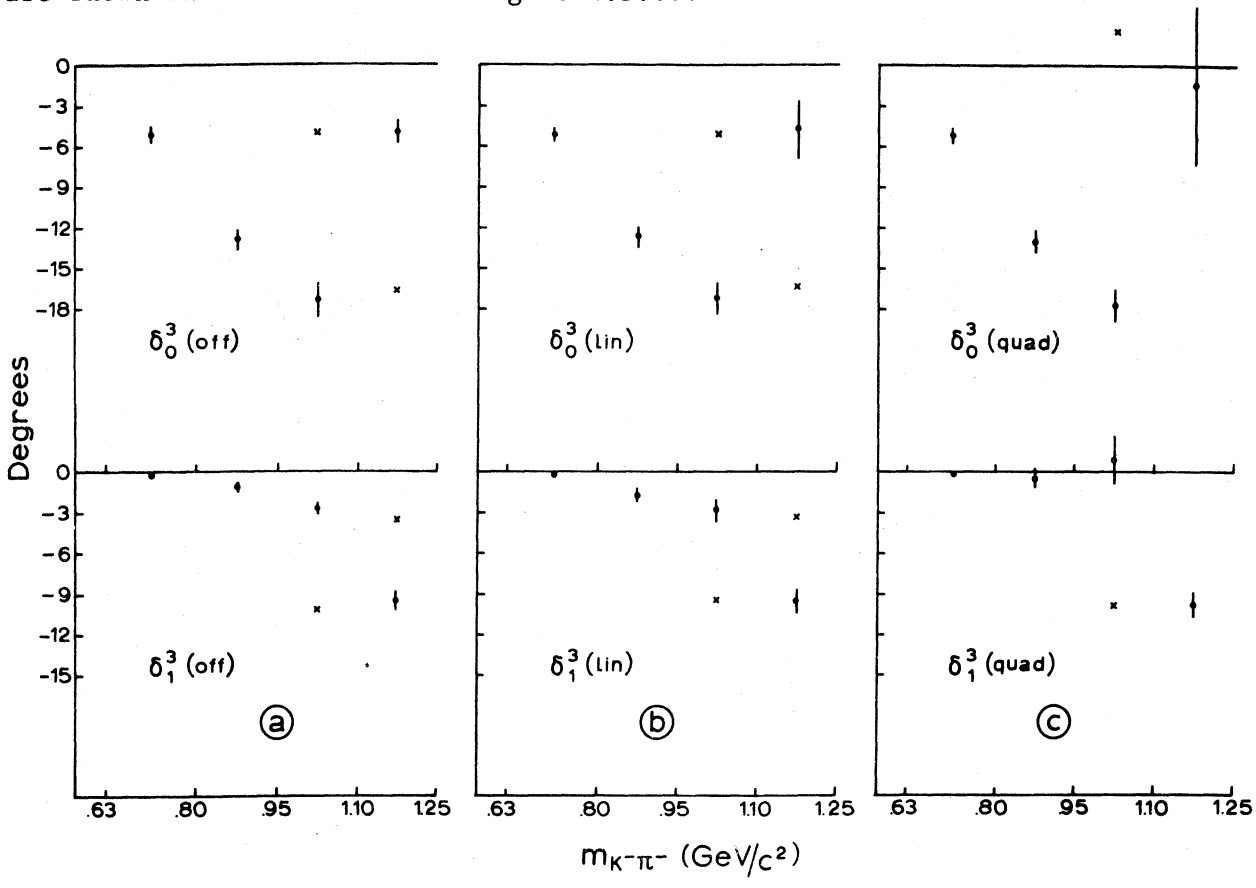

Fig. 4.5.11 The phase shifts δ_0^3 and δ_1^3 as a function of the $K^-\pi^-$ effective mass obtained from the on-mass-shell elastic $K^-\pi^-$ cross section and the

a. off-mass-shell moments;

b. linearly extrapolated moments;

c. quadratically extrapolated moments.

An inspection of the three tables 4.5.2 reveals that δ_0^3 is the same for non-extrapolated, linearly and quadratically extrapolated moments. The behaviour of δ_1^3 is also the same in the three cases, at least within two standard deviations. It may be remarked that in the case of quadratically extrapolation δ_1^3 is compatible with zero for $m_{K^-\pi^-} < 1.1$ GeV/c^2.

The ambiguity which has been found in the results for the phase shifts obtained with non-extrapolated moments in the two highest mass regions, appears also if the moments are linearly extrapolated. In the case of the quadratically extrapolated moments, the ambiguity appears only in the mass region

Table 4.5.2 Phase shifts for the I = 3/2 $K^-\pi^-$ elastic scattering in the reaction $K^- + p \to K^- + \pi^- + \Delta^{++}(1236)$, obtained from the on-mass-shell elastic $K^-\pi^-$ scattering cross section

a. with the off-mass-shell moments

$m_{K^-\pi^-}$ (GeV/c^2)	number of events	$-\delta_0^3$ (degrees)	$-\delta_1^3$ (degrees)	χ^2 (ND=1)	ambiguous solution $-\delta_0^3$ (degrees)	ambiguous solution $-\delta_1^3$ (degrees)	ambiguous solution χ^2 (ND=1)
< 0.80	314	5.1 ±0.5	0.3 ±0.1	0.4			
0.80-0.95	431	12.9 ±0.8	1.1 ±0.2	11.1			
0.95-1.10	486	17.3 ±1.2	2.7 ±0.4	40.2	5.1	10.0	90
1.10-1.25	293	4.9 ±0.8	9.5 ±0.9	20.4	16.6	3.7	54

b. with the linearly extrapolated moments

$m_{K^-\pi^-}$ (GeV/c^2)	number of events	$-\delta_0^3$ (degrees)	$-\delta_1^3$ (degrees)	χ^2 (ND=1)	ambiguous solution $-\delta_0^3$ (degrees)	ambiguous solution $-\delta_1^3$ (degrees)	ambiguous solution χ^2 (ND=1)
< 0.80	314	5.1 ±0.5	0.2 ±0.2	0.01			
0.80-0.95	431	12.7 ±0.8	1.7 ±0.5	0.18			
0.95-1.10	486	17.2 ±1.3	2.8 ±0.9	5.4	5.1	9.5	11.0
1.10-1.25	293	4.5 ±2.5	9.5 ±1.0	1.6	16.4	3.4	4.9

c. with the quadratically extrapolated moments

$m_{K^-\pi^-}$ (GeV/c^2)	number of events	$-\delta_0^3$ (degrees)	$-\delta_1^3$ (degrees)	χ^2 (ND=1)	ambiguous solution $-\delta_0^3$ (degrees)	ambiguous solution $-\delta_1^3$ (degrees)	ambiguous solution χ^2 (ND=1)
< 0.80	314	5.1 ±0.5	0.05 ±0.28	0.001			
0.80-0.95	431	13.0 ±0.8	0.5 ±0.8	0.65			
0.95-1.10	486	17.8 ±1.3	-1.0 ±1.9	0.48	-2.5	10.1	3.7
1.10-1.25	293	1.5 ±6.0	9.9 ±1.0	0.64			

Table 4.5.3 The values of $\sigma_{K^-\pi^-}$ (on-mass-shell), $\langle Y_1^0 \rangle$ and $\langle Y_2^0 \rangle$ (a: off-mass-shell, b: linearly extrapolated, and c: quadratically extrapolated) that have been used for the determination of the phase shifts, and the corresponding values calculated from the best fitted phase shifts.

a.

$m_{K^-\pi^-}$ (GeV/c^2)	$\sigma_{K^-\pi^-}$ (mb) input for fit	$\sigma_{K^-\pi^-}$ (mb) calculated with δ_0^3, δ_1^3	$\langle Y_1^0 \rangle_{off}$ input for fit	$\langle Y_1^0 \rangle_{off}$ calculated with δ_0^3, δ_1^3	$\langle Y_2^0 \rangle_{off}$ input for fit	$\langle Y_2^0 \rangle_{off}$ calculated with δ_0^3, δ_1^3
< 0.8	1.82 ±0.37	1.82	0.054 ±0.016	0.055	0.013 ±0.016	0.002
0.8-0.95	3.25 ±0.41	3.25	0.077 ±0.014	0.084	0.052 ±0.014	0.006
0.95-1.1	3.22 ±0.43	3.25	0.115 ±0.014	0.138	0.103 ±0.014	0.017
1.1-1.25	1.94 ±0.36	1.94	0.129 ±0.019	0.154	0.154 ±0.018	0.232

b.

$m_{K^-\pi^-}$ (GeV/c^2)	$\sigma_{K^-\pi^-}$ (mb) input for fit	$\sigma_{K^-\pi^-}$ (mb) calculated with δ_0^3, δ_1^3	$\langle Y_1^0 \rangle_{lin}$ input for fit	$\langle Y_1^0 \rangle_{lin}$ calculated with δ_0^3, δ_1^3	$\langle Y_2^0 \rangle_{lin}$ input for fit	$\langle Y_2^0 \rangle_{lin}$ calculated with δ_0^3, δ_1^3
< 0.8	1.82 ±0.37	1.82	0.031 ±0.029	0.031	0.004 ±0.031	0.001
0.8-0.95	3.25 ±0.41	3.25	0.120 ±0.030	0.123	0.026 ±0.031	0.013
0.95-1.0	3.22 ±0.43	3.22	0.119 ±0.039	0.143	0.106 ±0.039	0.019
1.0-1.25	1.94 ±0.36	1.94	0.120 ±0.068	0.143	0.158 ±0.064	0.235

c.

$m_{K^-\pi^-}$ (GeV/c^2)	$\sigma_{K^-\pi^-}$ (mb) input for fit	$\sigma_{K^-\pi^-}$ (mb) calculated with δ_0^3, δ_1^3	$\langle Y_1^0 \rangle_{quad}$ input for fit	$\langle Y_1^0 \rangle_{quad}$ calculated with δ_0^3, δ_1^3	$\langle Y_2^0 \rangle_{quad}$ input for fit	$\langle Y_2^0 \rangle_{quad}$ calculated with δ_0^3, δ_1^3
< 0.8	1.82 ±0.37	1.82	0.010 ±0.054	0.010	0.002 ±0.056	0.000
0.8-0.95	3.25 ±0.41	3.25	0.043 ±0.059	0.040	-0.046 ±0.059	0.001
0.95-1.0	3.22 ±0.43	3.22	-0.046 ±0.093	-0.052	0.067 ±0.094	0.002
1.0-1.25	1.94 ±0.36	1.94	0.065 ±0.226	0.049	0.414 ±0.205	0.250

$0.95 < m_{K^-\pi^-} < 1.10$ GeV/c^2. In this context it may be remarked that the quadratic extrapolation of the $\langle Y_2^0 \rangle$ moment in the mass region $1.10 < m_{K^-\pi^-} < 1.25$ GeV/c^2 is not very satisfactory. However, an inspection of the χ^2 (δ_0^3, δ_1^3) surface in this mass region makes the ambiguous solution also dubious in the case of the linearly extrapolated moments, as well as in the case of the off-mass-shell moments.

A larger sample of events is necessary to improve the results of the extrapolation. Then also the possible contribution of inelastic Kπ scattering may be determined as well as the possible contribution of higher order waves. This may also give more certainty about the ambiguities in the solution. The values of $\sigma_{K^-\pi^-}$, $\langle Y_1^0 \rangle$ and $\langle Y_2^0 \rangle$ calculated from the best fitted phase shifts are shown in table 4.5.3. In all three cases the calculated values of $\sigma_{K^-\pi^-}$ agree with the experimental values. In figure 4.5.10 the calculated values of the moments are also indicated by triangles.

4.5.7 EVIDENCE FOR A DOMINANT OPE MECHANISM

It has been found[4.26] in other experiments that the assumption of a dominant OPE mechanism, if necessary modified by form factors, for low four-momentum transfer, often gives a rather good description for reactions of the types

$$X + N \rightarrow X + \pi + N$$
$$\text{and} \quad X + N \rightarrow X + \pi + \Delta^{++}(1236) \qquad (4.5.4)$$

in which X stands for π, K, p or $\bar{p}$ particles and N for nucleons. Only reactions with charge-exchange are considered, to avoid difficulties from competing ω-exchange processes.

In the case of the present analysis of reaction 4.1.1, the assumption of a dominant OPE mechanism may be justified by the following arguments.

1. As remarked in section 4.2.4, the $K^-\pi^-$ Chew Low plot (fig. 4.2.3) for events of reaction 4.1.2, submitted to the condition on the $p\pi^+$ effective mass 4.2.4 in the region of the $\Delta^{++}(1236)$ resonance, shows a strong accumulation of events at low four-momentum transfer.

2. The formula 4.3.3, derived with the assumption of a dominant OPE mechanism, describes the behaviour of the experimental differential cross section of reaction 4.1.2 rather well (sect. 4.3.4).

3. The distribution of the Treiman Yang angle ϕ_K of the analysed events (fig. 4.4.2) is reasonable flat, as expected from a pure OPE. Here it may be

reminded that the distribution of ϕ_K, with a suppressed $K^*(890)$ background (fig. 4.5.4) is found to be more flat.

However, these arguments are far from a proof of the validity of a dominant OPE mechanism. More information may be obtained from the analysis of the scattering angles at the proton vertex and the comparison of this analysis with the results extracted from real $\pi^+ p$ scattering experiments.

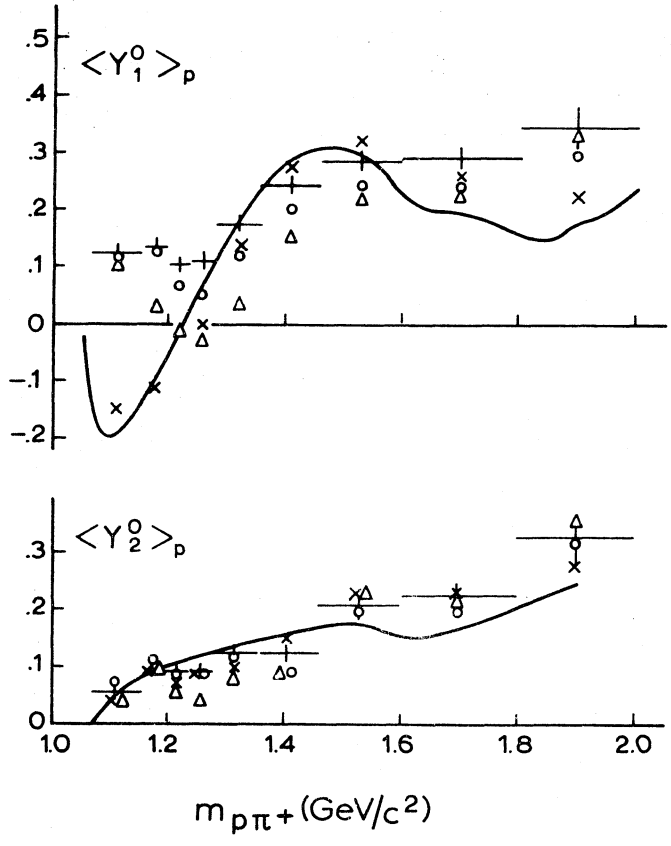

Fig. 4.5.12 Moments of the proton scattering angular distribution in the $p\pi^+$ rest system as a function of the $p\pi^+$ effective mass;

— off-mass-shell moments (with statistical errors) obtained in the present analysis, from events with $-t_{p \to p\pi^+} < 0.4$ (GeV/c)^2;

▵ idem and also $m_{K^-\pi^+\pi^-} < 1.2$ or $m_{K^-\pi^+\pi^-} > 1.5$ GeV/c^2;

o off-mass-shell moments with the events weighed as described in section 4.5.2;

x quadratically extrapolated moments obtained in the reaction $K^+ + p \to K^+ + \pi^- + \Delta^{++}(1236)$, reference 4.25.

The lines indicate the values calculated from the phase shifts determined in a real $\pi^+ p$ scattering experiment, reference 4.27.

Such an analysis has been done by Bingham et al.[4.25], using the data from the international K^+ collaboration in the reaction $K^+ + p \rightarrow K^{*o}(890) + p + \pi^+$. Making a cut in the $K^+\pi^-$ effective mass spectrum to select $K^{*o}(890)$-events, the moments of the $p\pi^+$ scattering angular distribution were determined for events satisfying the condition $-t_{p \rightarrow p\pi^+} < 0.3$ $(GeV/c)^2$. An extrapolation procedure with terms quadratic in $(t - \mu^2)$ was also applied in order to obtain the moments at the pion pole. As may be seen from figure 4.5.12 their extrapolated moments $\langle Y_1^0 \rangle_p$ and $\langle Y_2^0 \rangle_p$ are in reasonable agreement with the corresponding values obtained from the phase shifts determined in a real π^+p scattering experiment[4.27].

In the present analysis of reaction 4.1.1, the $p\pi^+$ off-mass-shell moments have also been determined for events obeying the condition $-t_{p \rightarrow p\pi^+} < 0.4$ $(GeV/c)^2$. The results are shown in table 4.5.4 and also in figure 4.5.12. Whereas the behaviour of the $\langle Y_2^0 \rangle_p$ moment of this experiment agrees very well with the result of Bingham, and the prediction from the real π^+p scattering, the $\langle Y_1^0 \rangle_p$ moment does not show this agreement, especially for values of the $p\pi^+$ effective mass below 1.24 GeV/c^2. By extrapolation of the moments to the pion pole the results were not improved. The moments $\langle ReY_1^1 \rangle_p$, $\langle ReY_2^1 \rangle_p$ and $\langle ReY_2^2 \rangle_p$ are compatible with zero as expected from a pure OPE.

It is investigated if this disagreement of the behaviour of the $\langle Y_1^0 \rangle_p$ moment at lower $p\pi^+$ effective masses may be caused by the presence of the Q(1300)-bump in the $K^-\pi^-\pi^+$ effective mass spectrum (fig. 4.5.13). According to a kinematical relation analogous to formula 4.5.2, the low $K^-\pi^-\pi^+$ effective masses in the region of the Q-bump are correlated with $\cos\theta_p \approx 1$. (θ_p is the angle between the outgoing and the incoming proton in the $p\pi^+$ rest system.) So events in which the Q(1300) is produced may contribute to the very large forward asymmetry in the $\cos\theta_p$ distribution of the sample analysed, which clearly results in a definite positive $\langle Y_1^0 \rangle_p$ moment over the whole $p\pi^+$ effective mass region considered.

This influence of the Q-bump is present as has been checked by determining the $p\pi^+$ moments of the events with $-t_{p \rightarrow p\pi^+} < 0.4$ $(GeV/c)^2$, and with the $K^-\pi^-\pi^+$ effective mass $m_{K^-\pi^-\pi^+} < 1.2$ or $m_{K^-\pi^-\pi^+} > 1.5$ GeV/c^2. Also the $p\pi^+$ moments are determined for the events with $-t_{p \rightarrow p\pi^+} < 0.4$ $(GeV/c)^2$, which have been weighed as described in section 4.5.2. This procedure reduces the influence of the $K^{*o}(890)$-events, and hence of the Q(1300)-events, which decay predominantly via the $K^{*o}(890)$ resonance (fig. 4.5.13).

The results of both subtractions of the Q-events are also shown in table 4.5.4 and sketched in figure 4.5.12. The behaviour of the $\langle Y_2^0 \rangle_p$ moment is hardly changed. The $\langle Y_1^0 \rangle_p$ moment is reduced somewhat, which corresponds to a

Table 4.5.4 The off-mass-shell moments $\langle Y_l^0 \rangle_p$ and $\langle Y_2^0 \rangle_p$ as a function of the $p\pi^+$ effective mass

$m_{p\pi^+}$ (GeV/c^2)	a. $-t_{p \to p\pi^+} < 0.4$ $(GeV/c)^2$ number of events	$\langle Y_l^0 \rangle_p$	$\langle Y_2^0 \rangle_p$	b. $-t_{p \to p\pi^+} < 0.4$ $(GeV/c)^2$ and $m_{K^-\pi^-\pi^+} < 1.2$ or > 1.5 GeV/c^2 number of events	$\langle Y_l^0 \rangle_p$	$\langle Y_2^0 \rangle_p$	c. $-t_{p \to p\pi^+} < 0.4$ GeV/c^2 and the events weighed by 1-BW(K^{*0}(890)) (sect. 4.5.2) weighed number of events	$\langle Y_l^0 \rangle_p$	$\langle Y_2^0 \rangle_p$
1.07-1.16	435	0.12 ±0.02	0.05 ±0.02	224	0.11 ±0.02	0.04 ±0.02	211.7	0.12 ±0.02	0.08 ±0.02
1.16-1.20	418	0.14 ±0.02	0.10 ±0.02	246	0.03 ±0.02	0.10 ±0.02	254.0	0.13 ±0.02	0.12 ±0.02
1.20-1.24	517	0.11 ±0.02	0.09 ±0.01	346	-0.01 ±0.02	0.06 ±0.02	307.0	0.07 ±0.02	0.09 ±0.02
1.24-1.28	328	0.11 ±0.02	0.09 ±0.02	198	-0.03 ±0.03	0.04 ±0.02	178.6	0.05 ±0.02	0.09 ±0.02
1.28-1.36	346	0.18 ±0.02	0.13 ±0.02	179	0.04 ±0.03	0.09 ±0.02	186.9	0.12 ±0.02	0.12 ±0.02
1.36-1.46	267	0.25 ±0.02	0.13 ±0.02	127	0.15 ±0.03	0.09 ±0.03	126.1	0.20 ±0.02	0.09 ±0.02
1.46-1.60	244	0.29 ±0.02	0.21 ±0.02	117	0.21 ±0.03	0.23 ±0.03	104.7	0.24 ±0.02	0.20 ±0.02
1.60-1.80	142	0.29 ±0.02	0.23 ±0.03	73	0.23 ±0.04	0.21 ±0.04	56.3	0.24 ±0.02	0.20 ±0.03
1.80-2.00	36	0.35 ±0.04	0.32 ±0.05	25	0.34 ±0.05	0.34 ±0.05	15.2	0.30 ±0.02	0.32 ±0.01

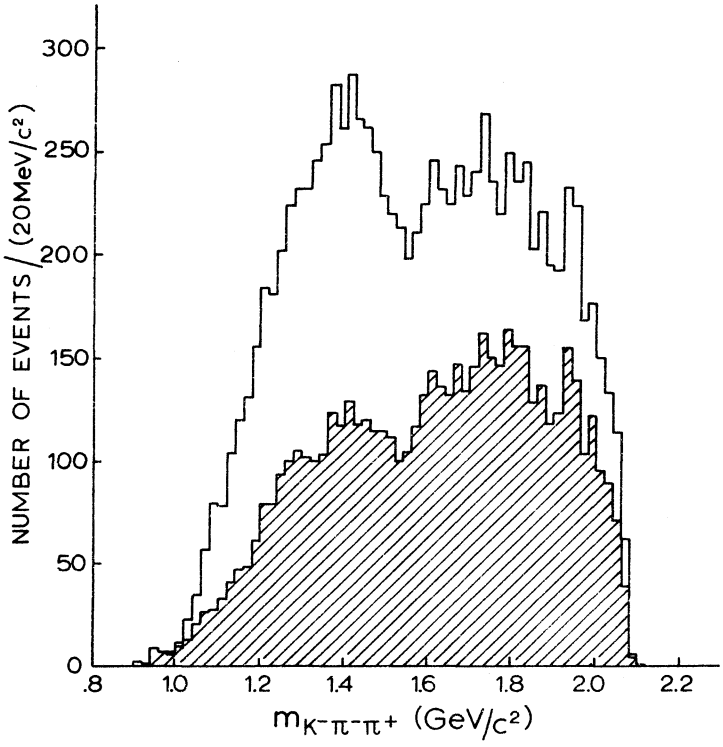

Fig. 4.5.13 The distribution of the $K^-\pi^-\pi^+$ effective mass in the reaction $K^- + p \to K^- + \pi^- + p + \pi^+$.
The shaded area indicates the distribution when the events are weighed with 1-BW(K^{*0}(890)) as described in section 4.5.2.

less forward asymmetric distribution of the cos θ_p. However, this effect is observed over the whole region of the $p\pi^+$ effective mass and not, or not especially, in the low $p\pi^+$ effective mass region.
In other experiments with different reactions of the type 4.5.4, an analogous behaviour of the off-mass-shell moments has been found[4.28]. So this attempt to extract evidence for a dominant one-pion-exchange is moderately successfull. The behaviour of the $\langle Y_1^0 \rangle_p$ moment is not understood. According to this fact it must be envisaged that the OPE model is not completely valid for the analysed reaction.

4.6 CONCLUSIONS

A sample of 39,000 four prong events was necessary to extract a sample of 1758 events suitable for the analysis of the isospin I = 3/2 $K^-\pi^-$ elastic scattering in the reaction

$$K^- + p \to K^- + \pi^- + \Delta^{++}(1236). \qquad (4.6)$$

The elastic $K^-\pi^-$ scattering cross section has been found to be about 2.7 mb for $K^-\pi^-$ effective masses up to 1.6 GeV/c^2 (table 4.3.3 and figure 4.3.4). This result agrees reasonably well with the results from other recent experiments[4.7] which are shown in figure 4.6.

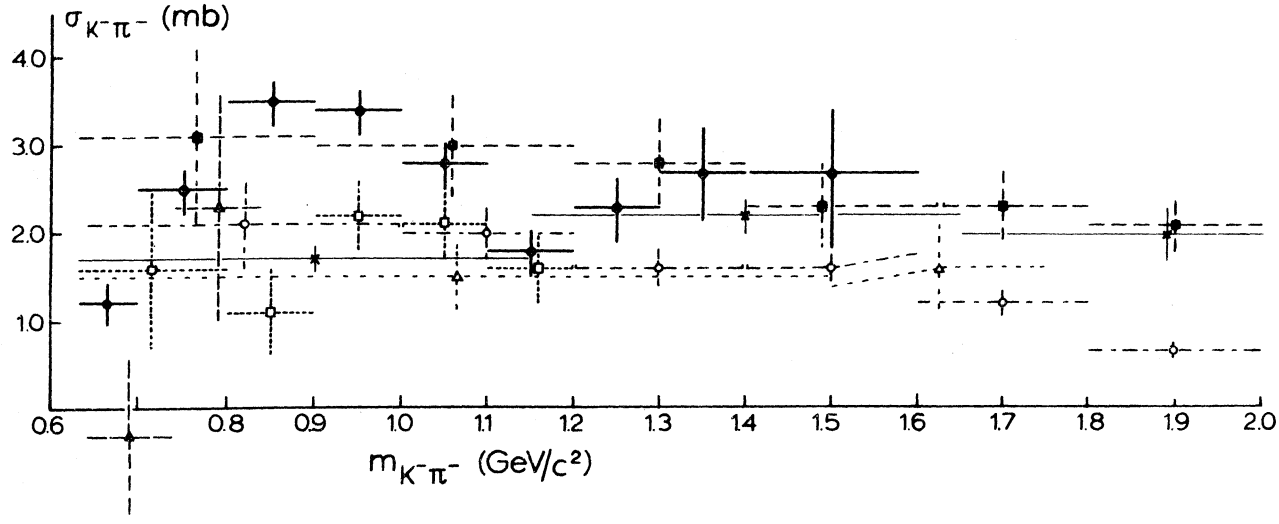

Figure 4.6 The results for the $K^-\pi^-$ elastic scattering cross section for $K^-\pi^-$ effective masses below 2.0 GeV/c^2 from Cho: o, Antich: ▵, Kirschbaum: ▲, Brankin: x, Bakker: □, Linglin: ■ (ref. 4.7) and the present work: ●.

The behaviour of the differential cross section $\frac{d\sigma}{dt}$ for the analysed sample is very well described by the used formula 4.3.3, with the order N of the expansion series being 2 (fig. 4.3.5).
The phase shifts δ_0^3 and δ_1^3 have been determined in a fit to the on-mass-shell elastic $K^-\pi^-$ scattering cross section and the spherical harmonic moments $\langle Y_1^0 \rangle$ and $\langle Y_2^0 \rangle$ of the scattering angular distribution of the K^- meson in the $K^-\pi^-$ rest system. Using the off-mass-shell moments, it has been found that $|\delta_0^3|$ increases from 5° for $m_{K^-\pi^-} < 0.8$ GeV/c^2 to 17° for $1.0 < m_{K^-\pi^-} < 1.1$ GeV/c^2 (table 4.4.2 and figure 4.4.6). In these regions of the $K^-\pi^-$ effective mass $|\delta_1^3|$ remains below 3°. For $1.0 < m_{K^-\pi^-} < 1.1$ GeV/c^2 the result is ambiguous with the solution $|\delta_0^3| = 5°$ and $|\delta_1^3| = 9°$. For $1.1 < m_{K^-\pi^-} < 1.2$ GeV/c^2 there

are also two ambiguous solutions $|\delta_0^3| = 4^o$ and $|\delta_1^3| = 9^o$ or $|\delta_0^3| = 15^o$ and $|\delta_1^3| = 3^o$. The last solution which has the smallest probability follows the behaviour of the phase shifts in the lower $K^-\pi^-$ effective mass regions. Both phase shifts δ_0^3 and δ_1^3 have the same sign. The sign can not be determined in this analysis because the formulas used 4.4.5 - 4.4.7 are invariant under a simultaneous change of sign for δ_0^3 and δ_1^3.

Suppressing the background processes did not significantly alter the results for the phase shifts.

Extrapolation of the moments does not substantially change the results for the phase shifts, except that in the case of quadratic extrapolation, δ_1^3 is compatible with zero for $m_{K^-\pi^-} < 1.1$ GeV/c^2 (table 4.5.2 and figure 4.5.11). The overall results are in good agreement with those of Bakker[4.23], whereas in his analysis quite different background effects are expected.

The spherical harmonic moments $\langle Y_1^0 \rangle_p$ and $\langle Y_2^0 \rangle_p$ of the scattering angle distribution of the proton in the $p\pi^+$ rest system have been determined in order to find evidence for the one-pion-exchange mechanism in the reaction 4.6. The behaviour of $\langle Y_2^0 \rangle_p$ agrees rather well with the experimental values obtained in a real π^+p scattering experiment. The deviating behaviour of $\langle Y_1^0 \rangle_p$ is not understood. An attempt to suppress the background due to the production of the Q(1300) did not yield an improved behaviour of $\langle Y_1^0 \rangle_p$.

A failure of the OPE model leads to a basic limitation of the validity of the extrapolation method.

A way of determining whether the poor representation of the moments of the $K^-\pi^-$ system by a s-wave and p-wave approximation is due to background processes or due to fundamental different processes that lead to the final $K^-\pi^-$ state may be repeating this analysis at other - preferably higher - incident K^- momenta.

REFERENCES

4.1. The results of the studies on resonances are regularly summarized by the Particle Data Group; see e.g., P.L. 39B (April 1972)

4.2. For survey papers see
Meson Spectroscopy, edited by C. Baltay and A.H. Rosenfeld; W.A. Benjamin, Inc. 1968
Proceedings of the Conference on ππ and Kπ Interactions; Argonne National Laboratory, May 1969, eds. Loeffler and Malamud
C.L. Kane: Critical Review of ππ and Kπ Scattering; Experimental Meson Spectroscopy, edited by C. Baltay and A.H. Rosenfeld; Columbia University Press 1970, p. 1
T.G. Trippe; Lawrence Radiation Laboratory, LBL - 763, preprint (1971)

4.3. D. Mettel; see ref. 4.2, LBL - 763, p. 12
P.E. Schlein; see ref. 4.2, Meson Spectroscopy, p. 161

4.4. H.H. Bingham et al.; N.P. B41 (1972) 1
R. Mercer et al.; N.P. B32 (1971) 381

4.5. T.G. Trippe et al.; P.L. 28B (1968) 203

4.6. P.E. Schlein; see ref. 4.2 "Argonne Conference", p. 458

4.7. E. Urvater et al.; P.R.L. 18 (1967) 1156
Y. Cho et al.; P.L. 32B (1970) 409
A.M. Bakker et al.; N.P. B24 (1970) 211
B. Jongejans and H. Voorthuis, Contribution to the International Conference on High Energy Physics; Kiev 1970 (Zeeman laboratorium, Internal report MP 109)
P. Antich et al.; N.P. B29 (1971) 305
J. Whitmore et al.; Bull. Am. Phys. Soc. 16 (1971) 547
A.M. Bakker; Contribution to the International Conference on Meson Resonances and Related Electromagnetic Phenomena; Bologna April 1971
B. Jongejans and H. Voorthuis; Contribution to the International Conference on Meson Resonances and Related Electromagnetic Phenomena; Bologna April 1971 (Zeeman laboratorium, Internal report 4.2 no 50)
A.R. Kirschbaum et al.; Lawrence Radiation Laboratory, UCRL-19426 Revised (1971), submitted to the Physical Review
C. Brankin et al.; Contribution to the Amsterdam International Conference on Elementary Particles (June 1971)
A.M. Bakker; Thesis (February 1972), Universiteit van Amsterdam
D. Linglin et al.; Ecole Polytechnique, LPNHE - 7.72 (01) (July 1972)

REFERENCES

4.1. The results of the studies on resonances are regularly summarized by the Particle Data Group; see e.g., P.L. 39B (April 1972)

4.2. For survey papers see
Meson Spectroscopy, edited by C. Baltay and A.H. Rosenfeld; W.A. Benjamin, Inc. 1968
Proceedings of the Conference on ππ and Kπ Interactions; Argonne National Laboratory, May 1969, eds. Loeffler and Malamud
C.L. Kane: Critical Review of ππ and Kπ Scattering; Experimental Meson Spectroscopy, edited by C. Baltay and A.H. Rosenfeld; Columbia University Press 1970, p. 1
T.G. Trippe; Lawrence Radiation Laboratory, LBL - 763, preprint (1971)

4.3. D. Mettel; see ref. 4.2, LBL - 763, p. 12
P.E. Schlein; see ref. 4.2, Meson Spectroscopy, p. 161

4.4. H.H. Bingham et al.; N.P. B41 (1972) 1
R. Mercer et al.; N.P. B32 (1971) 381

4.5. T.G. Trippe et al.; P.L. 28B (1968) 203

4.6. P.E. Schlein; see ref. 4.2 "Argonne Conference", p. 458

4.7. E. Urvater et al.; P.R.L. 18 (1967) 1156
Y. Cho et al.; P.L. 32B (1970) 409
A.M. Bakker et al.; N.P. B24 (1970) 211
B. Jongejans and H. Voorthuis, Contribution to the International Conference on High Energy Physics; Kiev 1970 (Zeeman laboratorium, Internal report MP 109)
P. Antich et al.; N.P. B29 (1971) 305
J. Whitmore et al.; Bull. Am. Phys. Soc. 16 (1971) 547
A.M. Bakker; Contribution to the International Conference on Meson Resonances and Related Electromagnetic Phenomena; Bologna April 1971
B. Jongejans and H. Voorthuis; Contribution to the International Conference on Meson Resonances and Related Electromagnetic Phenomena; Bologna April 1971 (Zeeman laboratorium, Internal report 4.2 no 50)
A.R. Kirschbaum et al.; Lawrence Radiation Laboratory, UCRL-19426 Revised (1971), submitted to the Physical Review
C. Brankin et al.; Contribution to the Amsterdam International Conference on Elementary Particles (June 1971)
A.M. Bakker; Thesis (February 1972), Universiteit van Amsterdam
D. Linglin et al.; Ecole Polytechnique, LPNHE - 7.72 (01) (July 1972)

4.8. G.F. Chew and F.E. Low; P.R. 113 (1959) 1640
4.9. R. Blokzijl et al.; N.P. B51 (1973) 535
4.10. G. Giacomelli; CERN - Hera 69-1
4.11. Particle data table (see e.g., P.L. 39B (April 1972)
4.12. G.G.G. Massaro; Zeeman laboratorium, Internal report 4.2 no 66 (December 1972)
4.13. CERN / D. Ph. II / Exp. 67-3
4.14. A.N.J.C. Lieshout; Zeeman laboratorium, Internal report 4.2 no 29 (November 1969)
4.15. Q.L.R.M. Merkies; Zeeman laboratorium, Internal report MP 107 (1970)
4.16. M.N. Focacci and G. Giacomelli; CERN 66-18 (1966), (Yellow report)
4.17. E. Ferrari and F. Selleri, N.C. 10 (1962) 453
4.18. H.P. Dürr and H. Pilkuhn; N.C. 40A (1965) 899
G. Wolf; P.R.L. 19 (1967) 925
J. Benecke and H.P. Dürr; N.C. 56A (1968) 269
4.19. A review of the results of several experiments is given by P.E. Schlein; see ref. 4.2, Meson Spectroscopy, p. 161
Z. Ming Ma et al.; P.R.L. 23 (1969) 342
4.20. D. Linglin; Thesis (1969), Faculté des Sciences d'Orsay, Université de Paris. (Copy: CERN / D Ph. II / Phys 69-34)
4.21. M.S. Bartlett; Phil. Mag. 44 (1953) 249
4.22. M. Ferro-Luzzi; CERN 68-23 (1968), (Yellow report)
4.23. A.M. Bakker; Thesis (February 1972), Universiteit van Amsterdam
4.24. H. Yuta et al.; P.R.L. 24 (1971) 1502
4.25. H.H. Bingham et al.; N.P. B41 (1972) 1
4.26. P.E. Schlein; see ref. 4.2 "Argonne Conference", p. 1
4.27. A. Donnachie et al.; P.L. 26B (1968) 161
4.28. E. Colton, et al.; quoted by Schlein; see ref. 4.2 "Argonne Conference" p. 1
E. Malamud et al.; Los Angeles report UCLA 1019 revised
T.G. Trippe et al.; P.L. 28B (1968) 203.

SUMMARY

In part A of this thesis a system is described in which three hand-measuring tables (Enetras) for the measurement of bubble chamber photographs operate on-line to a computer.
In Chapter 1 a survey is given of the process in a bubble chamber experiment before the measuring results - including the spatial and kinematic reconstruction - are ready for further analysis. The measurement equipment which had to be connected to the computer is described.
In Chapter 2 a survey is given of the configuration of the system with on-line measuring tables. Next the organization of the computer is described. An outline is given of the hardware necessary for the connection of the various units of a measurement device to the computer, including the automation of the transport of the bubble chamber photographs. A survey is given of the measuring process and the main computer programs to be used.
Basically the measurement proceeds as follows: The instructions for measurement are given by the computer to the operator of the measurement device via a telex machine. The measured coordinates are directly transferred to the computer. During measurement the computer sends diagnostics of errors to the operator, which may directly be rectified. If after the measurement of an event, the spatial reconstruction fails according to predetermined criteria, an instruction to remeasure the relevant event (completely or partially) is sent to the operator.
This system, in which the results of the measurement are directly processed in the computer so that unacceptable measuring errors may be immediately detected and rectified, has considerable advantages, the most important of which are summarized at the end of Chapter 2. The production per Enetra amounts to ± 6 measured events per hour, remeasurements being included.
In Chapter 3 the developed hardware is described in detail. This has mainly been done with the use of logic diagrams, for which the logic symbols are defined. Electronic specifications complete the logic diagrams. Special attention is given to the Brennermark reader which has been developed, for the purpose of counting the photographs when the film transport is controlled by the computer.

Part B of this thesis contains an analysis of the elastic scattering of π^- mesons to K^- mesons, which occurs in a pure isospin I = 3/2 state. Since these

particles are not available as static targets in the laboratory, the information has been extracted from the peripheral reaction $K^- + p \rightarrow K^- + \pi^- + \Delta^{++}(1236)$, where the momentum of the incoming K^- meson is 4.24 GeV/c.

A sample of 1758 events, which approximately accord with the above mentioned reaction, is obtained from the reaction $K^- + p \rightarrow K^- + \pi^- + p + \pi^+$, by selecting events with a low four-momentum transfer from the incoming K^- meson to the outgoing $K^-\pi^-$ system, and with a $p\pi^+$ effective mass in the $\Delta^{++}(1236)$ resonance region.

The experimental data have been obtained from a K^- meson exposure of the CERN 2m bubble chamber, filled with hydrogen. The K^- mesons with a momentum of 4.24 GeV/c were obtained, by electrostatic separation, from a secondary beam (m6) of the CERN proton synchroton. The experiment has been carried out in collaboration with the section High Energy Physics of the University of Nijmegen.

Information on the elastic $K^-\pi^-$ scattering may be obtained by extrapolation of observables as a function of the four-momentum transfer squared $t_{K^- \rightarrow K^-\pi^-}$ to the pole $t_{K^- \rightarrow K^-\pi^-} = \mu^2$, where μ is the mass of the π meson. It is assumed, that one-pion-exchange dominates in the reaction concerned at low four-momentum transfer.

The cross section of the elastic $K^-\pi^-$ scattering $\sigma_{K^-\pi^-}$ is determined by means of an extrapolation method based on suggestions of G.F. Chew and F.E. Low. The result, averaged over the region of the $K^-\pi^-$ effective mass considered is $\sigma_{K^-\pi^-} = 2.7$ mb. The formulas used give a satisfactory description of the differential cross section $d\sigma_{K^-p \rightarrow K^-\pi^-p\pi^+} / dt_{K^- \rightarrow K^-\pi^-}$ for the sample of events which has been analysed.

An attempt is made to determine the s- and p-wave phase shifts δ_0^3 and δ_1^3 of the elastic $K^-\pi^-$ scattering, with a one-constraint fit using the cross section $\sigma_{K^-\pi^-}$ and the "off-mass-shell" moments $\langle Y_1^0 \rangle$ and $\langle Y_2^0 \rangle$ at the K^- meson vertex. The absolute value of δ_0^3 increases gradually from 5^o for $m_{K^-\pi^-} < 0.8$ GeV/c^2 to 17^o for $1.0 < m_{K^-\pi^-} < 1.1$ GeV/c^2. In this mass region the absolute value of δ_1^3 remains below 3^o. For $1.1 < m_{K^-\pi^-} < 1.2$ GeV/c^2, $|\delta_0^3| = 4^o$ and $|\delta_1^3| = 9^o$. In the two highest mass regions there are two ambiguous solutions. A decision is not possible, mainly because of the large χ^2 of the fit. In the highest mass region the solution with the largest χ^2 is the one which accords the best with the behaviour of the phase shifts in the lower mass regions.

Refinements such as the subtraction of background and the extrapolation of the moments to the pole $t_{K^- \rightarrow K^-\pi^-} = \mu^2$ do not significantly alter the results.

In order to verify the dominance of the one-pion-exchange, the moments $\langle Y_\ell^m \rangle_p$ at the baryon vertex have been determined. The behaviour of $\langle Y_2^0 \rangle_p$, as a function of the $p\pi^+$ effective mass, agrees with the behaviour of the corresponding moment obtained from the phase shifts determined in a real $p\pi^+$ scattering experiment. The behaviour of $\langle Y_1^0 \rangle_p$ deviates from that of the corresponding calculated moment. Another criterion for a dominant one-pion-exchange, namely that the moments $\langle \mathrm{Re}Y_1^1 \rangle$, $\langle \mathrm{Re}Y_2^1 \rangle$ and $\langle \mathrm{Re}Y_2^2 \rangle$ are zero, is satisfied reasonably well, both at the baryon vertex and the K^- meson vertex.

SAMENVATTING

In deel A van dit proefschrift wordt een systeem beschreven waarbij drie met de hand bediende apparaten voor het uitmeten van bellenvat foto's (Enetra's) bestuurd worden door een rekenmachine.
In hoofdstuk 1 wordt een overzicht gegeven van de bewerkingen die bij een bellenvat experiment verricht moeten worden voordat meetresultaten beschikbaar zijn voor verdere analyse. De meetapparatuur, die beschikbaar was voor koppeling aan de rekenmachine, wordt beschreven.
In hoofdstuk 2 wordt een overzicht gegeven van de konfiguratie van het systeem met aangekoppelde meetapparaten. Vervolgens wordt de organisatie van de rekenmachine beschreven. Het principe van de elektronische schakelingen, nodig voor de aankoppeling van de verschillende delen van een meetapparaat aan de rekenmachine - w.o. de automatisering van het filmtransport - wordt uiteengezet. Een overzicht van het meetproces, met vermelding van de belangrijkste rekenmachine programma's wordt gegeven.
Schetsmatig verloopt de meetprocedure als volgt:
De meetopdrachten worden vanuit de rekenmachine aan de meetoperateur kenbaar gemaakt op een telex apparaat. De gemeten koördinaten worden onmiddellijk naar de rekenmachine gezonden. Tijdens het meten maakt de rekenmachine die fouten aan de meetoperateur kenbaar die direkt hersteld kunnen worden. Indien na de meting van een gebeurtenis de ruimtelijke rekonstruktie volgens van te voren vastgestelde kriteria faalt, ontvangt de meetoperateur opdracht tot het geheel of gedeeltelijk overmeten van die gebeurtenis.
Dit systeem, waarbij de meetresultaten, afkomstig van de meetapparatuur, direkt in de rekenmachine verwerkt worden, zodat eventuele ontoelaatbare meetfouten van de gemeten gebeurtenissen onmiddellijk gedetekteerd en gekorrigeerd kunnen worden, heeft aanzienlijke voordelen voor de meetproduktie. De belangrijkste voordelen worden opgesomd aan het einde van hoofdstuk 2. De opbrengst per Enetra is $\approx$ 6 - met spoorcentrering: $\approx$ 8,5 - gemeten gebeurtenissen per uur, inklusief het overmeten.
In hoofdstuk 3 worden de ontwikkelde elektronische schakelingen in detail beschreven. Dit gebeurt met behulp van logische diagrammen, waarvoor logische symbolen gedefiniëerd worden. Elektronische specificaties vullen de logische diagrammen aan. Speciale aandacht wordt geschonken aan de ontwikkelde Brennermark lezer, nodig voor het tellen van de foto's bij geautomatiseerd filmtransport.

In deel B van dit proefschrift wordt de analyse gegeven van het elastische verstrooiingsproces van π^- mesonen aan K^- mesonen, dat in een zuivere isospin

I = 3/2 toestand plaatsvindt. Aangezien deze deeltjes niet als statisch doelwit in het laboratorium ter beschikking zijn, is de informatie gezocht in de perifere reaktie $K^- + p \rightarrow K^- + \pi^- + \Delta^{++}(1236)$, waarbij het inkomende K^- meson een impuls heeft van 4,24 GeV/c.

Een verzameling van 1758 gebeurtenissen die bij benadering aan bovenstaande reaktie voldoen is verkregen uit de reaktie $K^- + p \rightarrow K^- + \pi^- + p + \pi^+$, door gebeurtenissen te selekteren met een lage vier-impuls overdracht van het inkomende K^- meson naar het uitgaande $K^-\pi^-$ systeem en met een $p\pi^+$ effektieve massa in het $\Delta^{++}(1236)$ resonantie gebied.

De experimentele gegevens werden verkregen uit een bestraling met K^- mesonen van het CERN 2 m bellenvat, gevuld met waterstof. De K^- mesonen met een impuls van 4,24 GeV/c werden middels elektrostatische separatie verkregen uit een sekundaire bundel (m6) van het CERN proton synchrotron. Het experiment is uitgevoerd in samenwerking met de afdeling Hoge Energie Fysica van de Universiteit van Nijmegen.

Informatie over elastische $K^-\pi^-$ verstrooiing kan verkregen worden door extrapolatie van gemeten grootheden als funktie van het kwadraat van de vier-impuls overdracht $t_{K^- \rightarrow K^-\pi^-}$ naar de pool $t_{K^- \rightarrow K^-\pi^-} = \mu^2$, waarbij μ de massa van het π meson is. Hierbij is aangenomen, dat in genoemde reaktie één-pion-uitwisseling domineert bij lage vier-impuls overdracht.

De werkzame doorsnede van de elastische $K^-\pi^-$ verstrooiing $\sigma_{K^-\pi^-}$ is bepaald met een extrapolatie methode die berust op suggesties van G.F. Chew en F.E. Low. Het resultaat, gemiddeld over het beschouwde gebied van de $K^-\pi^-$ effektieve massa $m_{K^-\pi^-}$, is $\sigma_{K^-\pi^-} = 2.7$ mb. De gebruikte formules geven voor de geanalyseerde verzameling van gebeurtenissen een goede beschrijving van de differentiële werkzame doorsnede $d\sigma_{K^-p \rightarrow K^-\pi^-p\pi^+} / dt_{K^- \rightarrow K^-\pi^-}$.

Getracht is de s- en p-golf fase verschuivingen δ_0^3 respectievelijk δ_1^3 van de elastische $K^-\pi^-$ verstrooiing te bepalen met een regressie van een vrijheidsgraad uit de werkzame doorsnede $\sigma_{K^-\pi^-}$ en de "off-mass-shell" momenten $\langle Y_1^0 \rangle$ en $\langle Y_2^0 \rangle$ aan het K^- meson vertex. De absolute waarde van δ_0^3 neemt geleidelijk toe van 5° voor $m_{K^-\pi^-} < 0.8$ GeV/c^2 tot 17° voor $1.0 < m_{K^-\pi^-} < 1.1$ GeV/c^2. In dit massa gebied blijft de absolute waarde van δ_1^3 onder de 3°. Voor $1.1 < m_{K^-\pi^-} < 1.2$ GeV/c^2 is $|\delta_0^3| = 4^\circ$ en $|\delta_1^3| = 9^\circ$. In de hoogste twee massa gebieden zijn tweeduidige oplossingen mogelijk. Een beslissing is niet mogelijk mede door de grote χ^2 van de aanpassing. In het hoogste massa gebied sluit de oplossing met de grootste χ^2 aan bij het gedrag van de fase verschuivingen in de lagere massa gebieden.

Verfijningen, zoals het aftrekken van achtergrond en de extrapolatie van de

momenten naar de pool $t_{K^-} \to K^-\pi^- = \mu^2$, geven geen duidelijke verandering in de resultaten.

Teneinde de dominantie van de één-pion-uitwisseling te verifiëren, zijn de momenten $\langle Y^m_\ell \rangle_p$ aan het baryon vertex bepaald. Het gedrag van $\langle Y^0_2 \rangle_p$, als funktie van de $p\pi^+$ effektieve massa, is in overeenstemming met de berekening afkomstig uit een reëel $p\pi^+$ verstrooiings experiment. Het gedrag van $\langle Y^0_1 \rangle_p$ wijkt af van deze berekening. Aan een ander kriterium voor een dominant één-pion-uitwisselings gedrag, nl. het nul zijn van de momenten $\langle ReY^1_1 \rangle$, $\langle ReY^1_2 \rangle$ en $\langle ReY^2_2 \rangle$, wordt zowel aan het baryon vertex als aan het K^- vertex redelijk voldaan.

ACKNOWLEDGEMENTS

Many individuals and organizations contributed to this work, and I would like to acknowledge my gratitude for the efforts that have made this work possible.

Having studied and worked in the field of low energy nuclear physics at the Vrije Universiteit in Amsterdam, I wish to thank all those who contributed to my training.

I am particularly grateful to Professor Dr. P. van Duijn for the encouragement he gave me as a young student.

Concerning the present work I thank in particular Dr. B. Jongejans for his cooperation: his valuable advice on matters concerning physics has undoubtedly improved this study. His willingness to read and comment upon the volume concerning electronics is most appreciated.

I am grateful to Mr. R.A. van Meurs for his assistence, and to Dr. G.F. Wolters and Dr. A.M. Bakker for reading and commenting upon the volume concerning physics.

I am very much obliged to Drs. R. Pfeiffers for taking great pains in checking the sections on electronics.

I wish to thank Mr. F.G. Nipperus for his help in developing the necessary hardware.

I greatly appreciate the cooperation in the 'Aankoppel' group, with Drs. A.A.J. Franken and Drs. Th. Bruins, Mr. H.H.J.M. Hermans, Drs. J.H.M. van den Bergh and Mr. N.R. Paasman.

My thanks are due to Mr. H.R. Schans for providing the figures for part B, and for his patient assistence in correcting the somewhat erratic photographic procedure in the figures for part A.

I am grateful for the electronic and technical assistence kindly offered by Mr. A.J. Baaijens, Mr. G.H.F. Kuiper and Mr. J.C.M. Stam.

I am indebted to Professor Dr. J.C. Kluyver, until recently director of the Zeeman laboratorium, for giving me the opportunity of undertaking this work.

My sincere thanks go to the supervisor of my thesis, Professor Dr. A.G.C. Tenner, whose critical remarks have been very valuable.

Thanks to all, too numerous to mention here, who were directly or indirectly involved in bringing this work to completion.